ELECTROCHEMICAL INVESTIGATION OF POWDER COATINGS AND THEIR APPLICATION TO MAGNESIUM-RICH PRIMERS FOR CORROSION PROTECTION

A Thesis
Submitted to the Graduate Faculty
of the
North Dakota State University
of Agriculture and Applied Science

By

Casey Roy Orgon

In Partial Fulfillment of the Requirements
for the Degree of
MASTER OF SCIENCE

Major Program:
Coatings and Polymeric Materials

May 2015

Fargo, North Dakota

North Dakota State University
Graduate School

Title

ELECTROCHEMICAL INVESTIGATION OF POWDER COATINGS AND THEIR APPLICATION TO MAGNESIUM-RICH PRIMERS FOR CORROSION PROTECTION

By

Casey Roy Orgon

The Supervisory Committee certifies that this ***disquisition*** complies with North Dakota State University's regulations and meets the accepted standards for the degree of

MASTER OF SCIENCE

SUPERVISORY COMMITTEE:

Dr. Dante Battocchi
Chair

Dr. Dean Webster

Dr. Andriy Voronov

Dr. Chad Ulven

Approved:

31st May 2015
Date

Dr. Dean Webster
Department Chair

ABSTRACT

Corrosion is the decomposition of metal and metal alloys which threatens the integrity of man-made structures. One of the more efficient methods of delaying the corrosion process in metals is by coatings. In this work, the durability of two polyester powder coatings were investigated for corrosion protection of AA-2024-T3. Polyester powder coatings crosslinked by either triglycidyl isocyanurate (TGIC) or β-hydroxyalkyl amide (HAA) compounds were prepared and investigated for barrier protection of metal substrates by electrochemical impedance spectroscopy (EIS). Polyester-TGIC coatings were found to provide better long-term protection, which can be attributed to the increased mechanical strength and higher concentration of crosslinking in the coating films. Additionally, the polyester powder coatings, along with a fusion bonded epoxy (FBE) were investigated for their compatibility as a topcoat for magnesium-rich primers (MgRP). Under proper application conditions, powder topcoats were successfully applied to cured MgRP while corrosion protection mechanisms of each system were maintained.

ACKNOWLEDGMENTS

I would like to take this opportunity to express my gratitude to Dr. Dante Battocchi, my thesis committee chair for all his help and guidance over the duration of my research at NDSU. In addition, I am grateful to my other thesis committee members, Dr. Dean Webster, Dr. Andriy Voronov, and Dr. Chad Ulven for their guidance and insight in helping me improve my research work. Also, Dr. Victoria Gelling for introducing me to coatings and electrochemistry, and playing a large part in my decision to pursue a graduate degree.

I would like to acknowledge the support of this research by the US Air Force under grant no. FA7000-13-2-0025. I would also like to thank the Valspar Corporation and the people I was able to work with in Minneapolis including Jeff Rogozinski, John Bronk, and Sam Decker for their guidance in teaching me as much as possible about powder coatings over a ten week period. Thanks to Scott Payne and Jayma Moore of the electron microscopy center for their help with SEM characterization. I am grateful to the students, staff, and faculty of the Department of Coatings and Polymeric Materials at North Dakota State University for all their input and guidance along the way.

Finally, I must express my greatest gratitude to my wife, Laura, for putting up with me for these years as a graduate student, and hopefully many more.

TABLE OF CONTENTS

LIST OF TABLES

LIST OF FIGURES

LIST OF SCHEMES

CHAPTER 1. ELECTROCHEMICAL INVESTIGATION OF TWO POLYESTER POWDER COATING CHEMISTRIES

Abstract

Two different polyester powder coating chemistries were investigated for corrosion resistance of AA-2024-T3 by barrier protection. The powder coating chemistries explored include polyester resins crosslinked by either triglycidyl isocyanurate (TGIC) or β-hydroxyalkyl amide (HAA) compounds. Powder topcoats were prepared as “fully formulated” systems, incorporating pigments and extenders, as well as “model coatings” prepared without the fillers. Cured coatings were characterized by thermogravimetric analysis (TGA), differential scanning calorimetry (DSC), dynamic mechanical analysis (DMA), and gravimetric water absorption. Coatings were applied and cured to AA-2024-T3, and exposed to constsnt immersion in 5% NaCl solution. Corrosion resistance by barrier protection was monitored by electrochemical impedance spectroscopy (EIS). Polyester topcoats crosslinked by TGIC compounds were found to provide increased protection to the aluminum substrate when compared to HAA crosslinked coatings. Polyester-TGIC coatings showed no adverse effects with the incorporation of pigments and extenders. In the polyester-HAA coatings, the presence of pigments and extender in the cured films cause a further reduction in time-duration of corrosion protection. The increased barrier protection provided by the polyester-TGIC systems, compared to the polyester-HAA coatings, can be attributed to higher mechanical strength and increased concentrations of crosslinking in the cured films.

Introduction

Corrosion Process

Corrosion, the degradation process of metals into metal oxides, can be both a boon and a burden. Many works of art or historic monuments and structures are viewed with an increased sense of prestige given by the decades old surface patina. Copper provides a unique look to antiquity with the turquoise green patina that develops with exposure. When present in structures designed for specific functions the effects of corrosion are not desired, and often dangerous. Degradation of structural members diminishes mechanical performance. Even with proper design and monitoring, corrosion leads to increased cost in protective systems and eventual part replacement. When underestimated, corrosion can lead to structural failures that threaten human life and safety.

Corrosion does not occur as a single chemical reaction. Instead, the process involves paired electrochemical half-cell reactions coupled by electron flow. At anodic reaction sites, metal solids are decomposed to metal ions and release electrons. Half-cell reactions producing electrons are oxidation reactions. Free electrons flow to cathodic sites to be consumed in the reduction reaction. Two reduction reactions are possible at cathodic sites with solution conditions dictating the dominant reduction reaction. In acidic solution the reduction of hydrogen ions to hydrogen gas is predominant. The dominant reduction reaction in neutral or basic solutions occurs with the reduction of dissolved oxygen to hydroxyl ions. The overall corrosion reaction is the sum of both half-cell reactions. An example for aluminum degradation in basic conditions is given by the following half-cell reactions:

$$Anode: \quad 4[Al(s) \rightarrow Al^{3+}(aq) + 3e^{-}]$$

$$Cathode: \quad 3[O_2 + 2H_2O + 4e^{-} \rightarrow 4OH^{-}]$$

$$Overall: \quad 4Al(s) + 3O_2 + 6H_2O \rightarrow 4Al^{3+} + 6\,OH^{-}$$

Reaction location at the metal surface depends on the heterogeneous nature of the metal. Grain boundaries, defects, and contamination can each alter local surface energy. Sites with higher surface energy are more likely to act as an anode, releasing metal ions into solution. A sketch of the complete corrosion process can be seen in Figure 1.1.

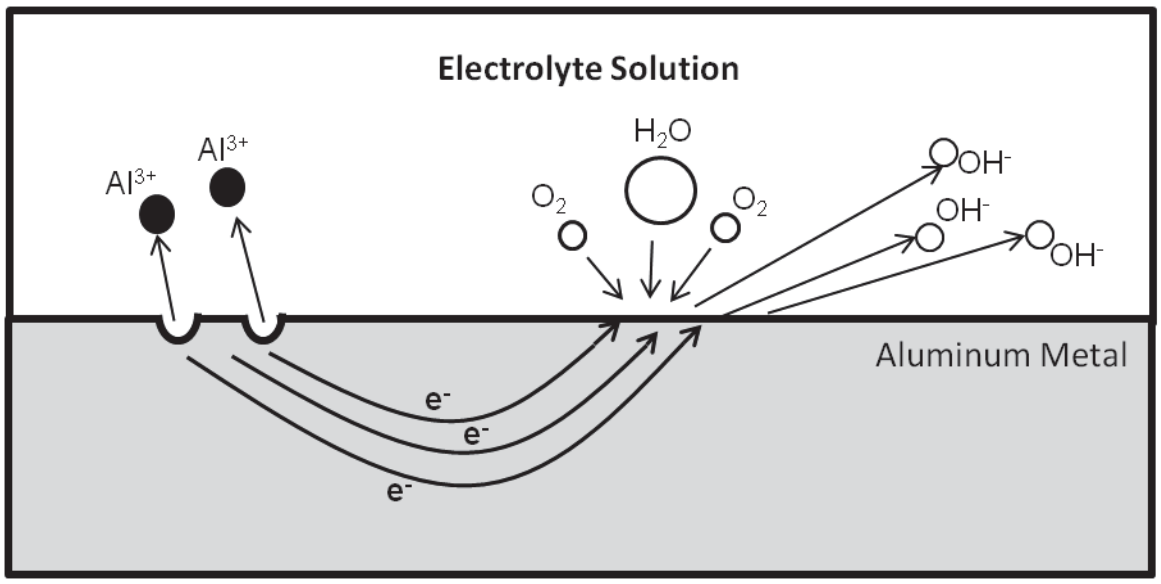

Figure 1.1. Sketch of corrosion process at an aluminum surface exposed to electrolyte.

In alloyed metals, reaction locations are strongly influenced by the distribution of reactive metal at the surface. Variation in surface composition creates a system susceptible to pitting corrosion, or localized degradation of active metal areas [1]. A well-studied example of pitting corrosion is exemplified by aluminum alloy 2024 [2-3]. Aluminum metal is highly active in terms of corrosion, but when in a pure form, can restrict corrosion by formation of a passive oxide film at the metal surface. Specific ions in electrolyte, usually Cl^-, can cause localized breakdown in the passive layer, exposing small areas of the metal surface for rapid oxidation [4] . This effect is amplified in alloyed metals, where precipitates of the alloying elements create surface abnormalities subject to pitting[5].

Protective Coatings

An effective means of limiting corrosion is provided by organic coatings. In addition to modifying color and appearance of structures or machines, coatings serve as a physical barrier between metal substrate and exposure environment. In terms of barrier properties, no coating will form a perfect barrier to corrosive environments as water, oxygen, and ions are all capable of penetrating organic films. To some degree, water penetration can be influenced by a number of effects, including diffusion due to concentration gradient, capillary action through voids, or osmosis driven by ion concentration gradient [6]. Degradation of coating performance has been demonstrated as a multistep process beginning with water and oxygen penetration into the film [7]. Underfilm corrosion begins when electrolyte has penetrated to metal surface, and cathodic and anodic reactions are initiated. Each reaction site creates a different environment for corrosion. Low pH conditions develop at anodic sites, attracting chloride ions and creating a cell prone to pitting corrosion. At cathodic locations the environment becomes highly basic, causing the coating to delaminate from the substrate. Overall barrier performance is influenced by factors including exposure environment, coating thickness, network properties, adhesion, and chemical degradation over time.

Coatings can be considered composite materials, as many are based on combinations of pigments and polymer resin. Often-times additives are included in coating formulations in order to modify specific characteristics. Before application, the uncured coating is suspended in solvent. Solvent functions as a means of material transfer, modifying viscosity for proper application, and serving as an aid in film formation and leveling. Once a uniform film is formed, solventborne coatings rely on the timely

evaporation of the solvent, allowing the film to coalesce and cure by desired mechanisms. Conventional organic solvents have proven efficient as transfer mediums, but the undesired effects of volatile organic content(VOC) on the environment has led to restrictions in their use [8].

Powder coatings provide one method of avoiding traditional solvents to create coatings free of VOCs. These systems are processed, stored, and applied as dry powders and do not require solvent at any stage. Raw materials are mixed as dry solids in flake, granule, or powder form. A homogeneous dispersion is created by processing the raw materials through extrusion, which melts the polymer resins and induces shear mixing by the extruder screws. In a solid state at room temperature, the material is further processed by grinding to fine powder particles. The powder is then sieved and classified to create a finished powder. Application of powder coats relies on particle fluidization by compressed air to transfer the coatings from bulk to thin powder layers. Curing the films at high temperatures allows the particles to melt, coalesce, and level to create a uniform film. The process also requires degassing of air present in the voids between particles before melting. Resins crosslinkable by many different chemistries have been adapted as powder coat systems can include epoxies [9-10], acrylics [11-14], polyurethanes [15-16], carboxylated polyesters [17-19], and siloxanes [15, 20].

Two chemistries used for crosslinking of carboxylated polyester resins are of particular interest, including triglycidyl isocyanurate (TGIC) and β-hydroxyalkyl amide (HAA) compounds. Polyester topcoats crosslinked by TGIC agents have been long recognized as superdurable topcoats for exposure applications [21-22]. The TGIC compound is a trifunctional crosslinker consisting of a triazine core with three epoxy-functional glycidyl branches. The reaction between resin and crosslinker occurs according to Scheme 1.1, where three carboxylic acid functional polyester chains, represented by P, react with the three epoxy functional groups of the TGIC molecule. Recent use of TGIC crosslinkers has been limited due to the potential for adverse health effect as noted by a number of organizations including the World Health Organization and European Union [21, 23].

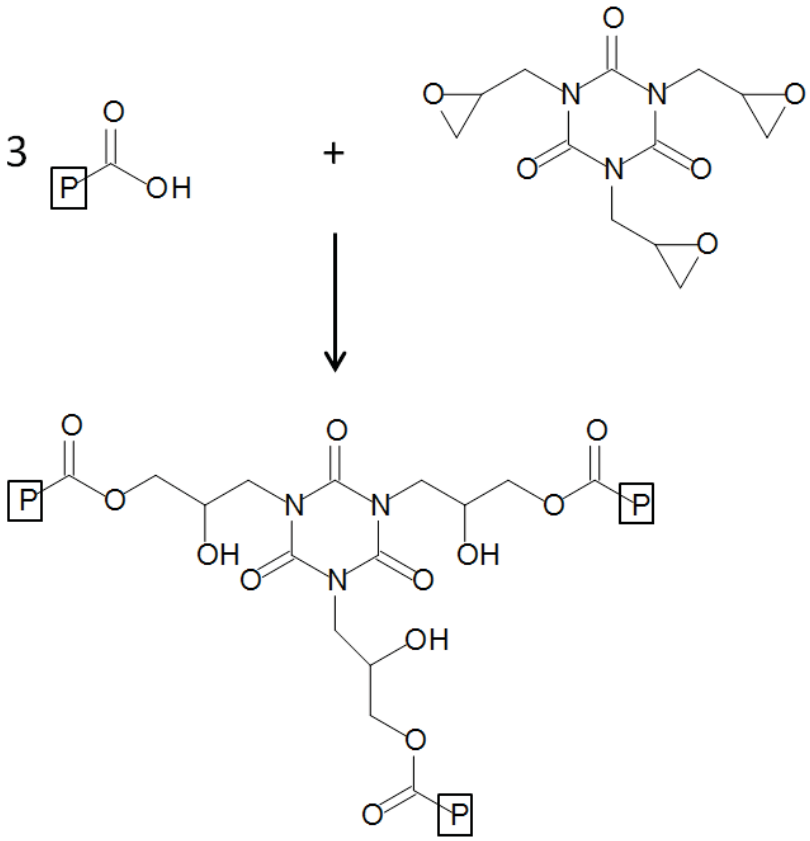

Scheme 1.1. Crosslinking reaction process between carboxylated polyesters and TGIC compounds.

To some extent the need for non-toxic crosslinking agent for polyester resins has been filled by the HAA compound, shown in the reaction scheme below, marketed by EMS-CHEMIE AG under the trade name Primid. Crosslinking occurs as a result of esterification between beta-hydroxyl alkyl amide groups from the crosslinker and carboxyl groups from the polyester chains. The reaction scheme occurs according to Scheme 1.2. In addition to chemical crosslinks, the reaction also produces water, which must be outgassed from the films in order to create a system free of voids. Water evolution limits film thickness, as water vapor creates voids and surface defects in thick-layer applications.

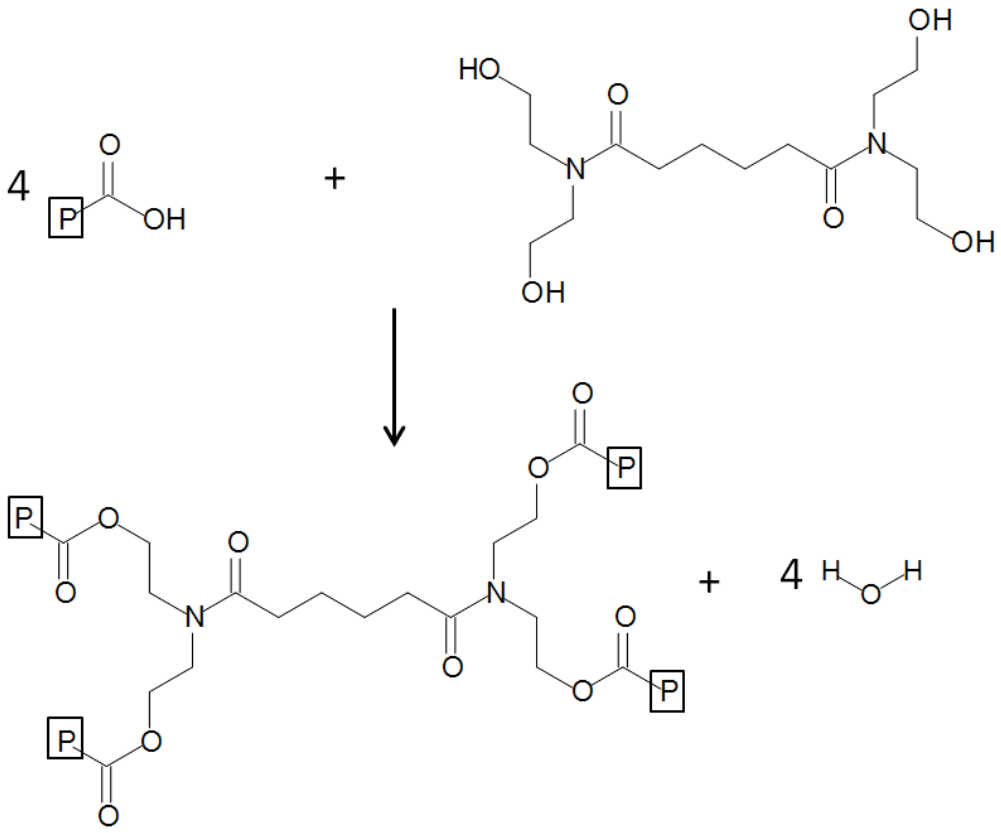

Scheme 1.2. Crosslinking reaction process between carboxylated polyesters and HAA compounds.

Protective coatings based on polyester resins crosslinked with either TGIC or HAA have been well studied in terms of thermal and mechanical properties. In comparison of the two chemistries it has long been accepted that TGIC exhibits superior outdoor durability [24], though published research comparing TGIC and HAA systems in similar exposure environments is limited [21]. In terms of weathering degradation, research has focused on replacement of terephthalic acid (TPA) with isophthalic acid (IPA) in the polymer backbone of polyester resins [19, 25]. While TPA based polyesters provide better mechanical properties, specifically flexibility, IPA based polyesters provide better stability to weathering. Monserrat et al determined TGIC systems exhibit greater stability under thermal aging than similar HAA crosslinked coatings [26]. Studies focused on varying crosslink agent content and cure cycles in order to determine resulting thermal, mechanical, and dielectric properties [18, 27-31]. Mafi et al has demonstrated the relationship between network properties and electrochemical barrier performance by comparison of epoxy/polyester and polyester coating chemistries [32].

A number of methods exist to evaluate weathering and exposure performance of topcoats. Investigation of chemical changes can be explored by infrared spectroscopy [33-35], nuclear magnetic resonance [36-37], electron spin resonance [38], and mass spectroscopy [39] techniques. Chemical analysis is often focused on the effects of UV radiation exposure. Results attained from chemical analysis can prove the validity of specific weathering tests [40] and provide insight to effective additives for light stabilization and absorption [41]. Cure response of thermosetting polymers influences final network properties, all of which can be characterized via thermal analysis by thermogravimetric and differential scanning calorimetric techniques [42-43]. Physical network behavior can be measured by dynamic mechanical analysis (DMA) to determine degradation effects on physical properties [44]. Combinations of the above techniques can be used to determine the extent of film degradation and possibly explain different mechanisms to failure of protective barrier properties, but none are capable of definitively measuring the physical barrier performance of the film.

Many electrochemical techniques have been developed to monitor the effects of corrosion. Electrochemical impedance spectroscopy has been proven to provide valuable insight to physiochemical barrier properties of polymer coatings applied to metals [45]. Experiments can be performed on single layer or multilayer coatings systems as free standing or applied films. Free film analysis isolates the behavior of the coatings while analysis of the same films applied to a substrate exhibit behavior of the film in addition to interactions between substrate and coating. Analysis of multilayer coatings systems gives insight to possible synergistic behavior between substrate, primer, and topcoat. Measurements can be interpreted to determine the effects of adhesion, water permeability, and corrosion resistance [46]. Best of all, results reveal both qualitative and quantitative behavior of the system, which can be modeled as simple R-C circuits.

Electrochemical Impedance Spectroscopy (EIS)

Immersed in electrolyte, an ideal coating for corrosion prevention allows no current flow through the film. Seen in Figure 1.2, the system is analogous to a parallel plate capacitor with the coating film acting as a dielectric material while the electrolyte and metal substrate represent parallel conductive plates. Increased immersion time allows for electrolyte diffusion into the coating, creating conductive pathways for current flow and causing degradation of the barrier protection provided by the coating film.

This process can be monitored and characterized by EIS analysis without interference or destruction of the sample [47-48].

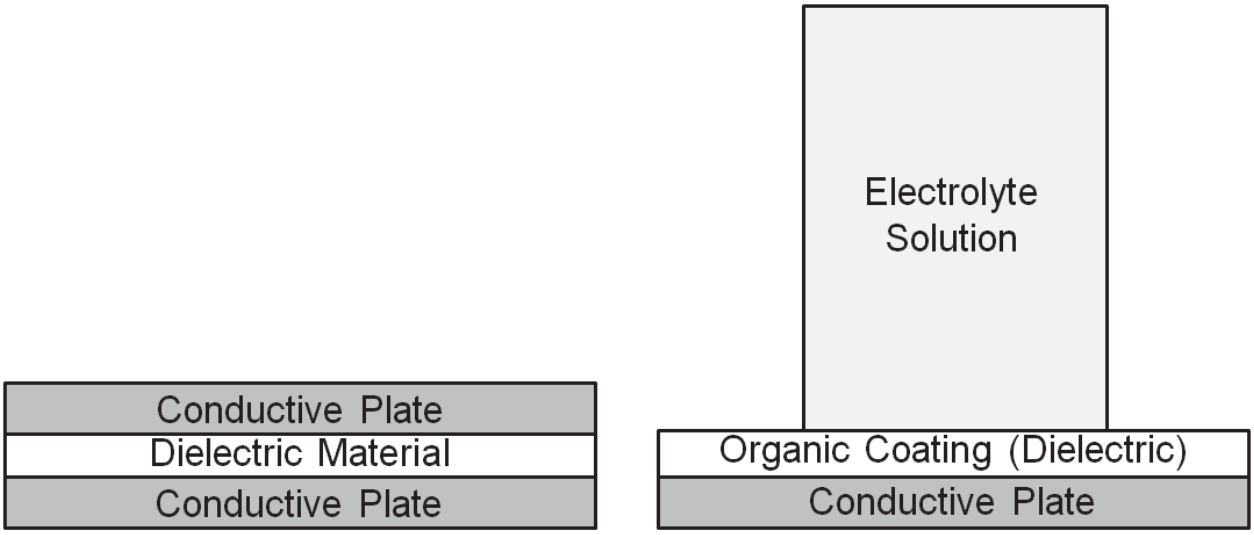

Figure 1.2. Similarities between parallel plate capacitor and electrochemical cell.

In direct current applications the resistance of an element can be determined by Ohm's Law:

$$V = RI \quad \text{(Eq. 1.1)}$$

Where V is voltage (volts), I is current (amps), and R is resistance (ohms). Using this similar principle applied with alternating currents (AC), EIS allows for characterization of both resistive and capacitive behavior. A small voltage perturbation, typically 10 mV AC, can be applied across the system

$$E(t) = E_o \exp(jwt) \quad \text{(Eq. 1.2)}$$

while measuring the resulting current response

$$I(t) = I_o \exp(j\omega t - \phi) \quad \text{(Eq. 1.3)}$$

to calculate the complex resistance, better known as impedance (Z)

$$Z(t) = \frac{E(t)}{I(t)} = Z_o(cos\phi + jsin\phi) \quad \text{(Eq. 1.4)}$$

where E(t) and I(t) are instantaneous voltage and current, respectively. Phase angle is represented by ϕ, which results from current lag or capacitive behavior in the system. Angular frequency is represented by ω, while j is the complex number. Being complex, impedance has both real and imaginary components, the effect of which depends on measured phase angle. Real components occur when θ=0° and are representative of one or more resistive elements in the system. Imaginary components occur at θ=-90°

and indicate the presence of capacitive elements. Coatings systems typically have a combination of both resistive and capacitive behavior, which changes with time due to exposure and degradation.

A common method of displaying EIS data is by the Bode plot, which separates impedance and phase shift into separate curves plotted versus frequency. Figure 1.3 shows theoretical behavior of a coating system at various stages of performance with Bode impedance and phase plots and Randle's cell circuit equivalents. Bode plots often combine impedance and phase curves into a single graph with multiple vertical axis. Both Z and ϕ are plotted with respect to frequency, usually in the range of 0.01-100,000 Hz. A coating that is providing perfect barrier protection to exposure is purely capacitive, represented in Figure 1.3(a), the impedance is shown as a linear down-sloping line while phase angle remains at -90°. Initial degradation of barrier properties will occur with diffusion of electrolyte into the film and are indicated by a decrease in impedance at low frequencies while phase angle approaches -45° (Figure 1.3(b)). Due to the effects of diffusion, it is favorable to replace coating capacitance (C_c) with a constant phase element (CPE), which has both magnitude and exponential variable (*n*). Capacitive behavior is observed at *n*=1, and as diffusion of electrolyte advances *n* approaches 0.5. As electrolyte diffuses further into the film conductive pathways are developed, eventually reaching the metal substrate. At this stage (Figure 1.3(c)) phase angle approaches 0° at mid-range frequencies and impedance plateaus in the low frequency region. Development of a pore resistance (R_p) is evidence of current flow through the film and, when measuring nonconductive barrier films, usually indicates the initiation of corrosion reactions at the substrate surface.

The presence of conductive pathways through the film creates additional processes in the system, as seen in Figure 1.3(d). Specific to cathodic reaction sites, increasing alkaline conditions can cause delamination of the coating, eventually creating blisters in the coating. With the metal surface in contact with electrolyte a monolayer of water molecules is adsorbed to the metal surface to create a dielectric layer. A negative charge builds at the metal surface, causing positively charged ions to assemble at the electrolyte surface of the double layer. In EIS results, this phenomenon is indicated by the presence of additional resistive and capacitive elements in data fitting. Double layer capacitance (C_{dl}) is the result of the non-conductive molecular monolayer at the metal surface. Charge transfer resistance (R_{ct}) is due to the physical transfer of electrons as a result of metal oxidation and species reduction when

electrolyte contacts metal. The presence of C_{dl} and R_{ct} are seen at lower frequencies where a second phase peak is developed along with a second plateau in the impedance curve. At this stage the coating is essentially failed. Advanced delamination and blister growth will eventually cause a rupture in the film, allowing bulk electrolyte direct contact with the substrate for corrosion.

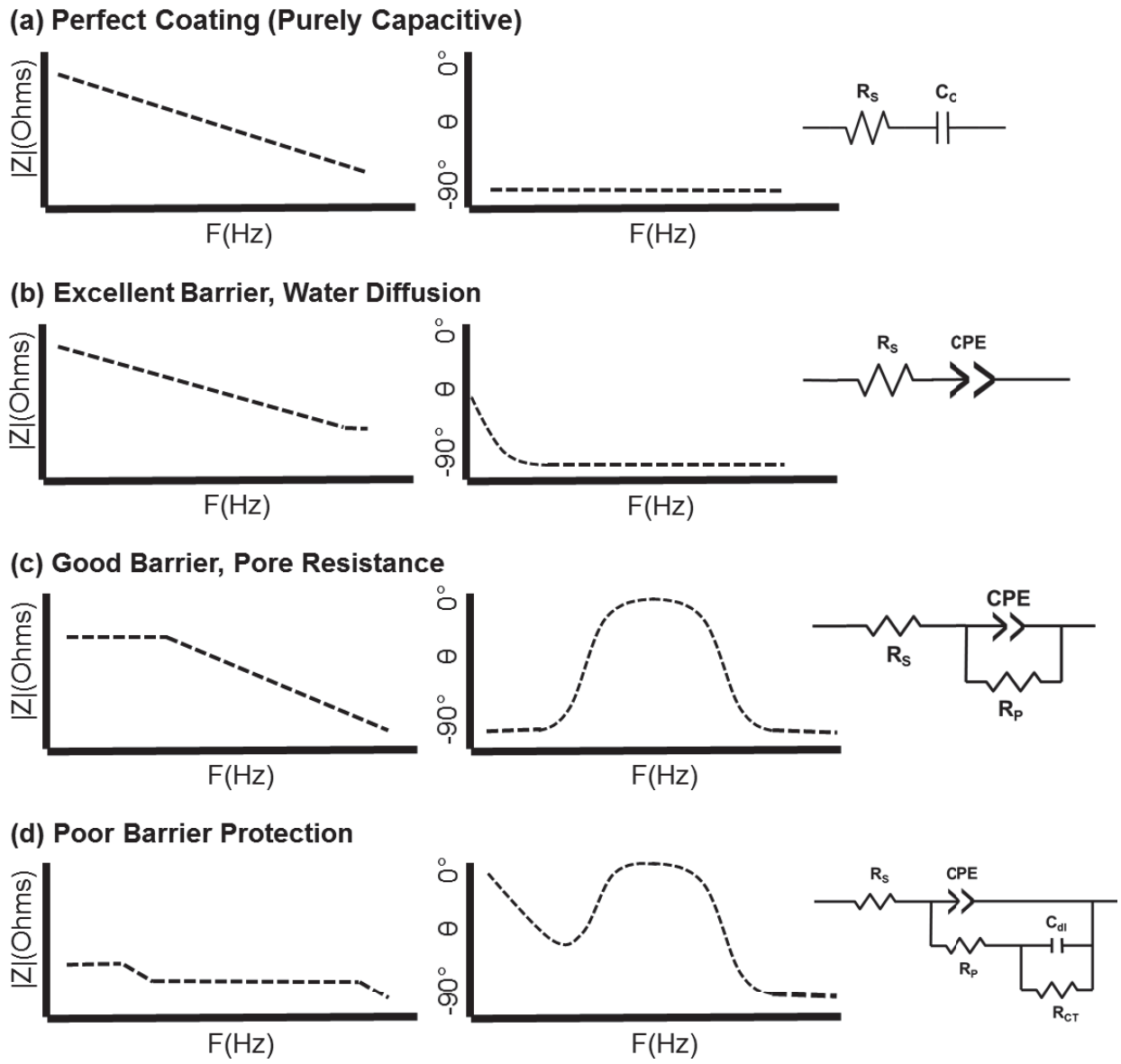

Figure 1.3. Bode impedance plots and Randle's cell equivalents for (a) ideal coatings, (b) coating subject to electrolyte diffusion, (c) coating with complete electrolyte penetration, (d) failed coating behavior.

Experimental

Powder Coat Preparation

Powder coatings used in this project were prepared according to the formulations listed in Table1.1. Formulations were varied by both crosslink chemistry and pigment concentration. Model systems, denoted by "MC" in the suffix of the formulation name, were produced to determine a baseline performance for non-pigmented coatings based on each of the crosslink chemistries. Addition of pigments and extenders in the fully formulated (FF) coatings allows for the characterization of the resin-crosslinker systems under the presence of non-crosslinkable inclusions in the film. Resin-crosslinker ratios of 90/10 for the polyester-TGIC and 95/5 for polyester-HAA are consistent with standard formulation ratios used for industrial manufacture of these powder chemistries. Small amounts of flow agent and degassing agents were added to all formulations. Pigmented coatings were prepared with barium sulfate extender and titanium dioxide as the primary pigment in addition to a small amount of colored pigments.

Table 1.1. Powder topcoat formulation information.

Formulation	Resin (R)	Crosslinker (X)	R-X Ratio (%wt)	PVC
PHMC	Polyester	HAA	95/5	0%
PHFF	Polyester	HAA	95/5	7.5%
PTMC	Polyester	TGIC	90/10	0%
PTFF	Polyester	TGIC	90/10	7.5%

Powders were prepared in batches of approximately four pounds. Raw material blends were made by combining resin, crosslinking agent, additives, extender, and pigments. Premixing was performed by manual agitation of the raw material blends. Material compounding was performed on a Coperion ZSK twin-screw powder coat extruder at a temperature of 120°C and 200 rpms. After passing through chill rollers, the extrudate was collected and manually pulverized to dime-size chips. Grinding was performed with a MIKRO Bantam hammer and screen mill. Material collected after grinding was sieved on a SWECO vibratory screening separator with a 150 mesh sieve to collect particles smaller than 100 µm for the finished paint powder. Finished powder was verified for batch consistency by gel time and visual appearance.

Coating Application

Aluminum panels were prepared from 150x75x2 mm^3 AA 2024-T3 panels, supplied by Q Panel Lab Products. Bare panels were prepared by sandblasting with 80 μm alumina grit and degreased with hexanes. Before powder coat application, cleaned panels were suspended in a preheated oven for 30 minutes with the oven set to the required cure temperature for the powder coating. Coating powders were added to the fluidized bed hopper and the air supply was increased until the powder was properly fluidized, resembling simmering water. The powders were allowed 30 minutes of fluidization before any panels were coated. Coatings were applied by fully immersing the preheated panels into the fluidized powder for approximately two seconds to build proper film thickness. The coated panels were then removed from the fluidized powder and placed back in the preheated oven for the recommended time to cure. Cure conditions and film build for each formulation are listed in Table 1.2. Cured panels were removed from the oven and allowed to air cool. Free films were prepared following a similar procedure with steel panels cut from a non-stick baking sheet. These panels were consistent in size with the aluminum test panels. Once cooled, these panels allowed for easy release of the cured free films.

Table 1.2. Powder topcoat recommended cure information.

Formulations	Gel Time	Cure Temperature (°C)	Cure Time (min)	Recommended Thickness (μm)
PHMC/PHFF	100s@ 175°C	175	10	50-75
PTMC/PTFF	100s@ 205°C	205	10	50-100

Thermogravimetric Analysis (TGA)

Thermal decomposition of the coatings was investigated by TGA using a TA Instruments Q500. Samples were prepared by adding approximately 10 mg of uncured powder to a 100 μL platinum pan. Experiments were performed from room temperature to 600ºC at 20ºC/min ramp rate and under nitrogen gas purge at 50 mL/min. Decomposition Temperature (T_d) was determined at 5% weight loss of the sample.

Differential Scanning Calorimetry (DSC)

Thermal behavior and extent of cure was characterized by conventional DSC using a Q1000 DSC from TA Instruments. Samples of cured free films were prepared by adding approximately 10 mg of

material to a standard aluminum DSC pan. Before DSC experiments were performed, residual thermal stresses were relieved by conditioning the samples in an oven at 50°C for 30 minutes. Heat-Cool-Heat cycles were performed from 25ºC to 250ºC at ramp rates of 20ºC/min for heating and 10ºC for cooling. Glass Transition Temperature (T_g) was recorded at the midpoint of the endothermic shift in the DSC curve.

Dynamic Mechanical Analysis (DMA)

DMA was performed using a TA Instruments Q800 DMA to investigate thermal behavior of the materials. Samples were prepared as fully cured coating free films cut to approximately 25.4mm long by 5mm wide and 0.1 mm thick. The prepared samples were conditioned at 50ºC for one half-hour to relieve any residual stresses. Experiments were run under strain-amplitude control of 0.01% with a preload force of 0.01 N and force track of 125%. Tests were conducted from room temperature to a final temperature of 200ºC at a ramp rate of 2ºC/min. A fixed frequency of 1 Hz was used for all tests. Measurement of storage modulus (E') and loss modulus (E") allowed for calculations of loss tangent (tan δ). The temperature at maximum tan δ was recorded as T_g. The E' at 60ºC above T_g was recorded as the rubbery plateau modulus (E_r), which was used to calculate crosslink density (υ) of the cured films by:

$$\upsilon = \frac{E_r}{3RT} \quad \text{(Eq. 1.5)}$$

where R is the universal gas constant (8.314 $cm^3PaK^{-1}mol^{-1}$) and T is absolute temperature (K). Due to pigment present in the system, crosslink density was calculated with Er modified by Guth's equation, assuming spherical pigment particles [49]:

$$E = E_o(1 + 2.5\phi + 14.1\phi^2) \quad \text{(Eq. 1.6)}$$

where E is the elastic modulus of the pigmented coating, E_o is the modulus of the unpigmented coating, and ϕ is the pigment volume fraction.

Water Absorption

Samples were prepared for gravimetric water absorption experiments by cutting square sections approximately 25.4 mm x 25.4 mm from cured coating free films of thickness 75±10 μm. The samples were cleaned with ethanol and dried overnight at room temperature. Initial mass was recorded and the samples were fully immersed in 18 MΩ Millipore ultra pure water at room temperature. Samples were immersed in a vertical upright position. At various time intervals, samples were removed from water,

carefully dried, and weighed. The scale used for measurements was a Mettler Toledo AB104-S with 0.1 mg accuracy.

Electrochemical Impedance Spectroscopy (EIS)

EIS studies were performed using Gamry Reference 600 Potentiostats with Gamry Framework Version 6.20/EIS300 data acquisition software. An electrolyte solution of 5% NaCl was used for all experiments and measurements were carried out in triplicates. Coatings applied to aluminum substrates were tested with a standard three electrode setup with a saturated calomel reference electrode, platinum mesh counter electrode, and the coated substrate as a working electrode. The electrochemical cell was contained by a glass cylinder clamped to the sample with an o-ring sealing the connection and preventing any leakage. The exposed area of the working electrode was 7.06 cm^3. Measurements were taken over a frequency range of 100,000-0.01 Hz with 10 collection points per frequency decade. An AC potential perturbation was applied at 10 mV RMS versus the open circuit potential of the system. All impedance data presented is normalized to 1 cm^2. Constant immersion samples were left uncovered at room temperature. Solution levels were monitored and, under the assumption that no salts would evaporate from the solutions, electrolyte levels were maintained by adding DI water until the original fill volume was achieved. At two week intervals the electrolyte solutions were flushed and replaced by new solution.

Results and Discussion

Thermal Analysis of Cured Films

Thermal stability of all powder formulations was investigated using TGA. Thermal analysis was performed on uncured powder samples to ensure cure reactions do not cause release of VOC's, indicated by weight loss of the sample. Decomposition temperature (T_d) was defined as 5% weight loss from the original sample mass. Results, displayed in Figure 1.4, show thermal degradation to be consistent between the two polyester powder chemistries. The pigmented polyester-HAA formulation showed the lowest T_d at 318°C. With recommended cure for each system at or below 200°C, it is safe to assume VOC's for these systems negligible and cure temperatures for the coatings are not sufficient for material degradation over these short time intervals (<10 min). The overall order of decomposition is PHFF<PTFF<PHMC<PTMC occurring over the temperature range of 318-355°C. Results show little change between the TGIC and HAA chemistries in terms of decomposition. The presence of pigments in

the coatings has a more influential effect on degradation. Both fully formulated systems, which each contain ~7.5% pigment by volume, show a decrease in T_d of approximately 20°C when compared to the corresponding model coating.

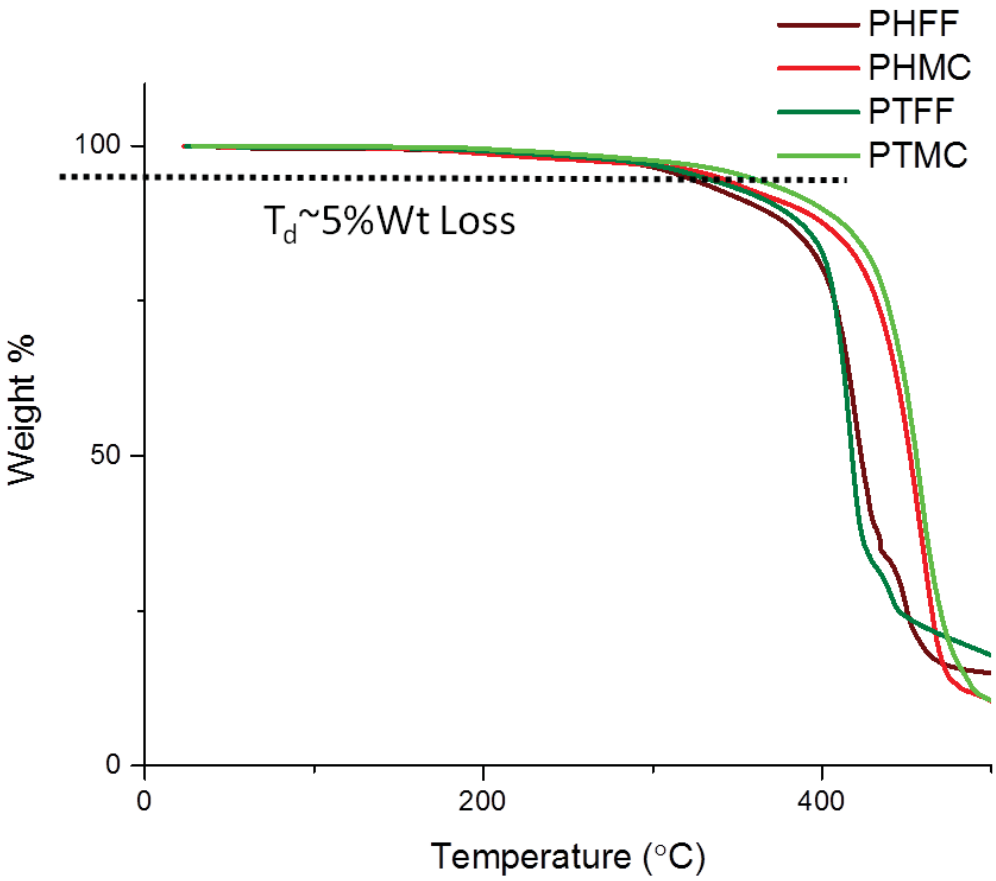

Figure 1.4. Thermogravimetric analysis results for each of the polyester powder topcoats.

Thermal events from DSC analysis are shown in Figure 1.5. Coatings were tested after subjecting them to their respective recommended cure cycles. Results shown are from a second heat cycle, performed immediately after cooling from a heat ramp up to the cure temperature for each formulation (listed in Table 1.2). This initial heating was done to allow the annealing of residual stresses in the samples. The time at elevated temperatures in fact, would be relatively short when compared to cure schedules that each sample had already undergone. The second heat ramp displays glass transition temperature (T_g) while the first ramp allows for determination extent of cure. Fully cured coatings were defined as exhibiting no endothermic process following T_g. Results show that the cure cycle

recommended for each of the four systems is sufficient to complete the cure of the films, as the curves for each sample maintain a linear path after the glass transition. First cycle results for each coating are not shown, as there were no significant thermal events observed, and the T_g is better determined from the second heat ramp.

It is important to keep in mind that this method of characterization classifies the functional cure of the system. It is possible that unreacted functional groups remain in the films, but the polymer networks have crosslinked to the point that any unreacted functional groups lack the mobility to meet and react with an opposing unreacted group.

A clear distinction can be seen between crosslink chemistries with the DSC results. During the heating ramp T_g appeared as the characteristic shift of the DSC curve in the endothermic direction. Results from the HAA systems were consistent, despite pigment concentration, with T_g occurring at approximately 65.5°C.Transition variation between PHMC and PHFF was less than 0.5°C, which was

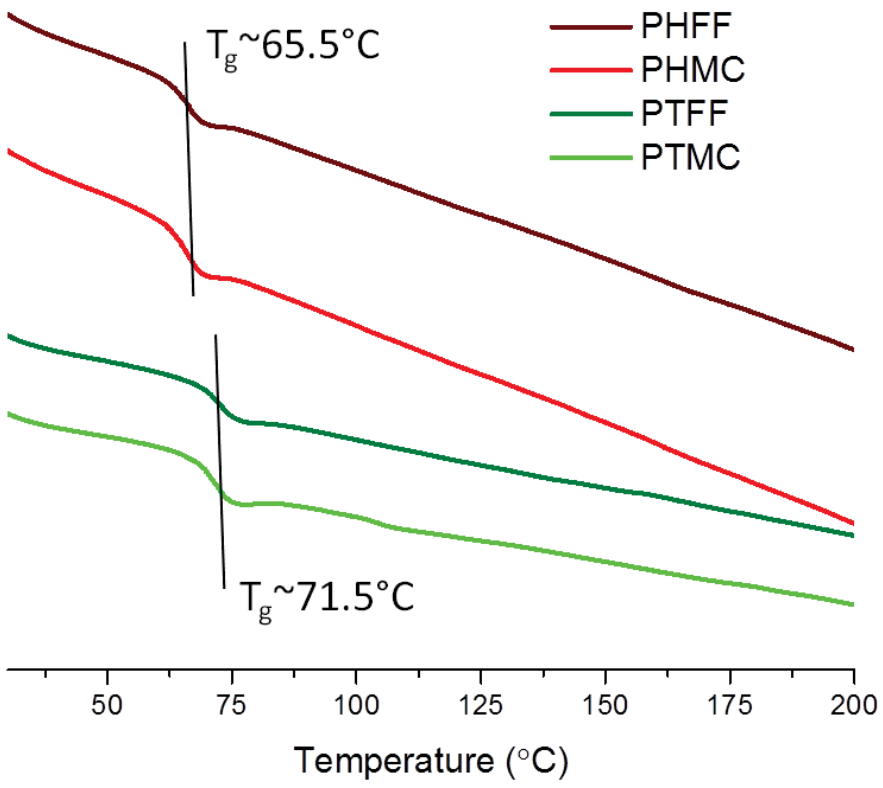

Figure 1.5. Differential scanning calorimetry results for each of the polyester powder topcoats.

considered insignificant in view of variations in samples mass and instrument error. A post-transition enthalpy relaxation peak is slightly distinguishable with PHMC, indicating a small increase in internal stress when compared to PHFF. A higher glass transition was exhibited in TGIC crosslinked formulations. Again, pigment concentration showed little effect on T_g, observed at 71.5°C for both pigmented and unpigmented systems. The pigmented system PTMC showed a slight relaxation peak following T_g, consistent with what was exhibited by PPMC.

Effects of pigment concentrations in coatings has been well documented [50]. Specific to T_g, pigment particles effects are influenced by the type of bonding between particles and binder. Pigmented coatings are often modeled as a three-phase system including the bulk polymer matrix, pigment particles, and an inter-phase consisting of adsorbed binder at the matrix-particle interface. It is possible for pigment effects to decrease T_g or leave it unchanged, but in most cases an increase in T_g is exhibited with increasing pigment concentration. Rigid amorphous inter-phase polymer chains are constrained by adsorption and effectively limit the mobility of nearby chain segments [51]. Although small, the enthalpic relaxation exhibited in both MC-formulations indicates the increased mobility of polymer chains in these systems compared to FF-formulations. The presence of pigments does not appear to have significant effects on T_g with either polyester crosslinking chemistry. Concentrations of pigment volumes in both FF-systems is relatively low at <8% by volume.

The effect of temperature on mechanical behavior was observed by DMA investigation. Storage modulus (E') and Tan Delta (tan δ) curves for all four coating systems are displayed in Figure 1.6 between the temperatures of 50°C and 180°C. All samples were tested as fully cured free films, verified by DSC results, in the film tension instrument setup. Being fully cured, only three stages of behavior should be prominent in the curves. These stages include amorphous glassy behavior, visco-elastic region around the glass transition, and finally the rubbery elastic state. Storage modulus in the rubbery plateau was used to calculate crosslink density of the films. Free films for all formulations tested performed consistent with this assumed behavior. In the glassy state, E' was relatively high as molecular vibration of chain segments was restricted. At the onset of glass transition storage modulus began a steady decrease, indicating increasing molecular motion in the polymer networks. Again, samples showed

relatively good curing, as E' showed no significant increase after T_g, indicating no further crosslinking reactions. This further reinforces results from DSC trials verifying film cure.

The T_g was recorded at maximum tan δ or E"/E', shortly after which the storage modulus leveled out again to rubbery elastic behavior. At approximately T_g+60°C rubbery behavior was consistent across all formulations and E' at this temperature was recorded and used in calculations involving crosslink density. In both chemistries, the fully formulated systems exhibit higher E' in the glassy region. This effect is presumably due to the relatively high modulus of minerals used as pigments and extenders. DMA results show a very distinct difference between the TGIC and HAA crosslinked chemistries. The overall behavior is consistent between formulations but the magnitudes of both E' and tan δ are noticeably greater with the TGIC crosslinked systems. Values for Tg and E' are listed in Table 1.3 along with calculated crosslink density. Pigment effects were taken into consideration for crosslink density calculations, and E' was modified by Guth's equation (Eq.1.6) assuming good adhesion between pigment and binder. It was also assumed that at f=1 Hz the oscillation frequency was sufficiently low for E' to be consistent with Young's modulus (E). Comparison of the two crosslink chemistries is very interesting. With four reactive –OH groups, the HAA molecules have a higher functionality than the TGIC molecules. It could be expected that this would allow HAA-based chemistries to achieve a higher storage modulus and crosslink density than TGIC. Results show the opposite to be true. Though the functionality is higher, it is possible that this chemistry does not react to the same extent as the TGIC systems. This would contribute to the increased presence of unreacted –OH groups in the polymer film.

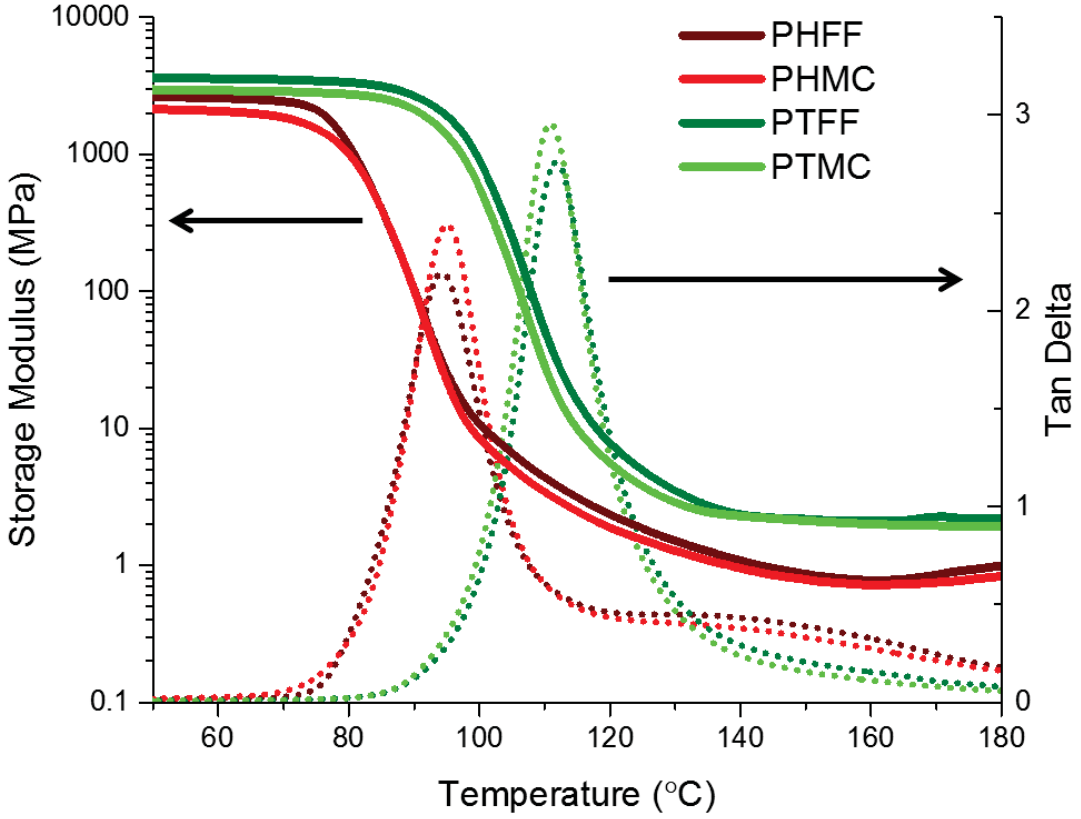

Figure 1.6. Dynamic mechanical analysis results for each of the polyester powder topcoats.

Table 1.3. Storage modulus and calculated crosslink densities of the polymer films.

	Tg+60 [°C]	E' [Mpa]	v [mol/cm^3]
PHMC	155	1.091	1.19E-4
PHFF	154.2	1.301	1.12E-4†
PTMC	170.9	2.116	2.21E-4
PTFF	172	2.139	1.76E-4†

†-Calculated using E' adjusted for pigment effects by Eq 1.6.

Another consideration must be made to the physical structure of the crosslinking molecules, shown in Figure 1.7. TGIC is a compact molecule including a triazine ring at the core with three short glycidyl branches. Even at high thermal energy levels the molecular structure limits mobility of the segments. The HAA compound is an H-shaped molecule with four short hydroxyl functional branches. The middle section of the molecule is comprised of a pair of nitrogen atoms separated by a short hydrocarbon chain. Considering molecular structure and mobility of the "core" section of each crosslinking agent, it is logical that the TGIC compound limits molecular mobility to a greater extent than HAA. This effect would result in increased storage modulus of TGIC crosslinked systems in comparison to the HAA crosslinking agent.

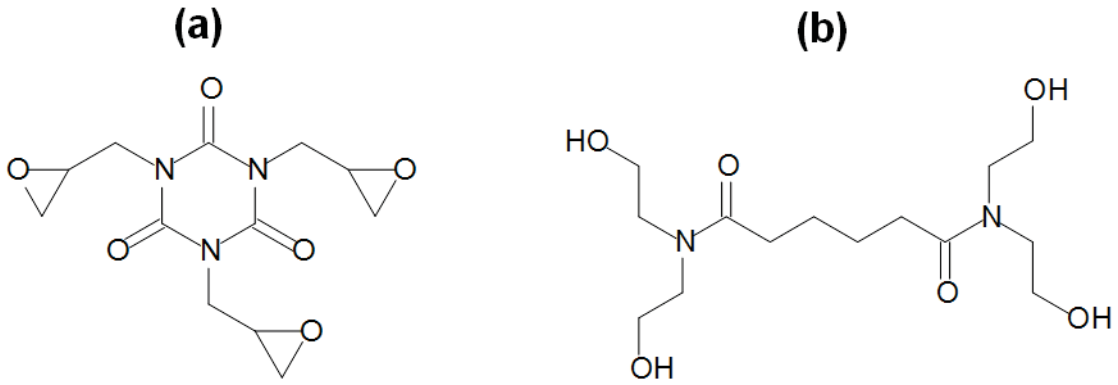

Figure 1.7. Structures of (a) TGIC crosslinker and (b) HAA crosslinker for carboxylated polyester resins.

Free film samples, approximately 1 in^2, were immersed in ultra-pure water to determine water absorption into the films at room temperature. Absorption was calculated as the total weight gain for each sample with respect to time. Results shown in Figure 1.8 are consistent with the expected behavior of the polymer films. Initially after immersion, the water content in the films increased rapidly, before eventually leveling off and remaining nearly constant thereafter. Initial water diffusion is rapid as the water molecules fill unoccupied space in the polymer networks. Swelling of the film causes polymer chains to extend. Absorption slows when polymer chains are fully extended and no free volume remains for further diffusion of water. This scenario is assumed for pure polymer networks.

The presence of pigments, extenders, and additives can lead to more complex behavior. Results from each of the TGIC crosslinked systems are similar. Over the first 100 hours of immersion, the films increased in weight by approximately 1.1% due to water absorption. Out to almost 1200 hours immersion the water uptake was about 1.3%, indicating slowed absorption rates as water molecules saturated the films. Consistency in weight gain results between pigmented and unpigmented TGIC crosslinked formulations shows this chemistry to be very stable in immersion. Presence of pigments and extenders does not appear to change the behavior of the networks in terms of water uptake. After DMA trials, it was assumed that HAA-crosslinked network would allow for greater water uptake by the films when compared to the TGIC chemistry. In fact, both PHFF and PHMC displayed less water absorption when compared to their corresponding TGIC system. In addition, there was a clear distinction with the presence of pigments; model coat HAA samples showed increased water absorption when compared to the PHFF system, and was assumed that this is due to the lack of water absorption by the pigment and extender particles. Titanium dioxide and barium sulfate, both present in the FF systems, are known to be practically insoluble in water.

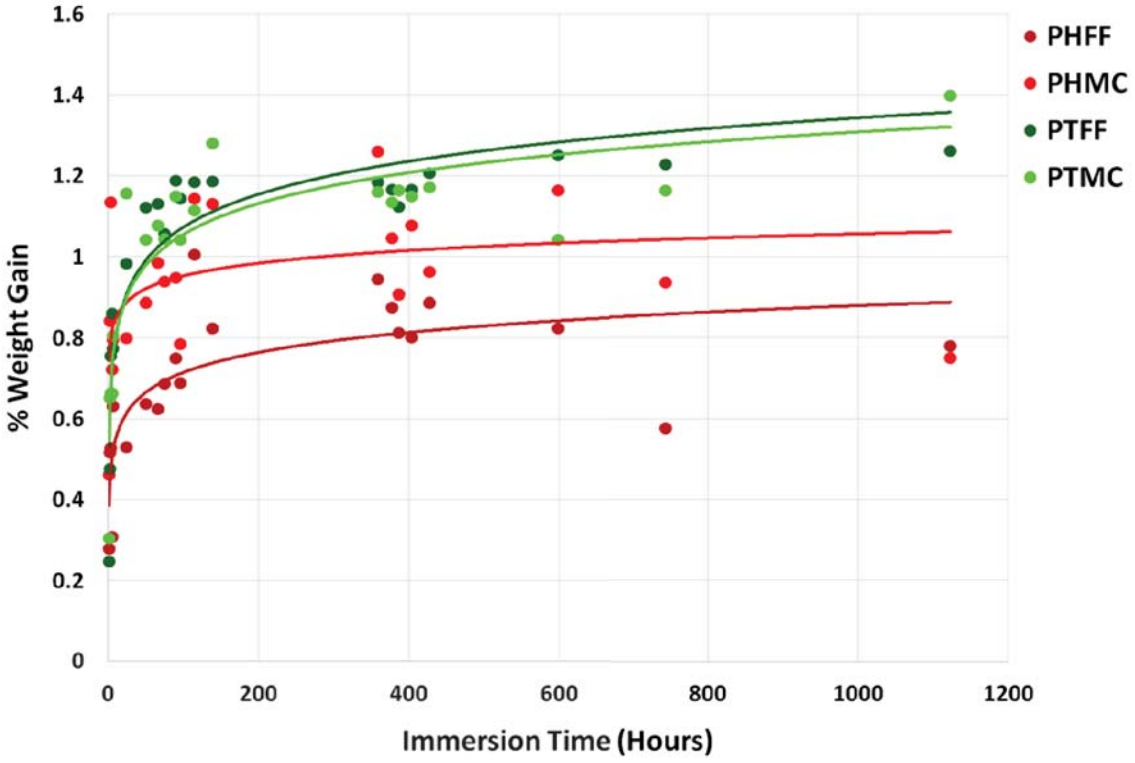

Figure 1.8. Water absorption of polyester free films.

It is possible the pigment particles are limiting water absorption by two mechanisms, first occupying volume that could otherwise be filled by water molecules. And a second effect could be the decreased mobility of the polymer chains adsorbed to or near the particles. Further examination of results from the HAA systems shows another inconsistency when compared to the TGIC systems. As immersion time increased the PTFF and PTMC formulations achieved a stable weight gain percentage. Increasing immersion time for both PHFF and PHMC results shows a decrease in weight gain. Over the first 100 hours PHMC data follows closely with the TGIC formulations. PHFF and PHMC show maximum water absorption around 400 hours where weight gains are at 0.9% and 1.1% respectively. Near 1200 hours immersion water uptake for each has decreased to 0.8% for both HAA crosslinked systems. Currently, the cause for weight loss observed in the HAA crosslinked systems is not fully understood.

Electrochemical Investigation of Barrier Properties

Barrier properties of the polyester powder topcoats were characterized by EIS. This technique allows for both qualitative and quantitative assessment of material behavior. At early stages of exposure, diffusion of electrolyte into the films is observed. High impedance and phase angle measurements near -90° indicate the material is behaving almost fully capacitive, allowing no measureable current flow through the film. Diffusion of water into the film is noted by a slight decrease in impedance while the phase angle approaches -45°.

The rate of diffusion can be correlated with the polymer network structure and crosslink density. It is assumed that a rigid network high in crosslink density is favorable for resistance to electrolyte diffusion into the film. Increasing exposure times allow for further penetration by the electrolyte, which will eventually progress through the film to interact with the metal substrate. Upon contact between electrolyte and substrate, conductive pathways are developed between the metal and exposure environment, effectively initiating the corrosion process. At this stage a decrease in low frequency impedance is observed along with the phase shift approaching 0° at mid-range frequencies. Conductive pathways allow for current flow and the film exhibits parallel capacitive and resistive behavior. Values for equivalent circuit models of all systems exposed by constant immersion to 5% NaCl have been compiled in Table 1.4.

Table 1.4. Values for circuit model elements for each topcoat formulation at various immersion times.

Time (Hours)	Circuit Model*	CPE	n	R2	C_{dl}	R_{ct}
PTMC						
0	(b)	5.19E-10	0.993			
500	(c)	4.13E-10	0.990	2.14E+10		
1000	(c)	4.25E-10	0.988	5.88E+09		
2500	(c)	4.99E-10	0.972	6.13E+08		
4000	(c)	5.26E-10	0.967	8.15E+08		
PTFF						
0	(b)	3.18E-10	0.992			
500	(c)	3.73E-10	0.983	3.19E+10		
1000	(c)	3.81E-10	0.982	1.55E+10		
2500	(c)	3.80E-10	0.982	5.41E+09		
4000	(c)	3.81E-10	0.983	4.74E+09		
PHMC						
0	(b)	3.09E-10	0.998			
1000	(c)	3.56E-10	0.986	5.55E+09		
1500	(c)	3.44E-10	0.989	1.71E+09		
2500	(c)	4.08E-10	0.974	1.36E+07		
4000	(d)	5.50E-10	0.956	2.18E+06	1.34E-07	5.04E+06
PHFF						
0	(b)	3.98E-10	0.994			
500	(c)	4.38E-10	0.993	9.52E+09		
1000	(c)	4.91E-10	0.985	3.94E+06		
2500	(d)	4.45E-10	0.996	2.65E+05	1.99E-06	8.69E+05
4000	Failed	5.55E-10	0.981	2.80E+05		

*Refer to Figure 1.3 for corresponding circuit models

Despite initial corrosion processes at the electrolyte-substrate interface the metal is not necessarily unprotected. As long as current flow is sufficiently low, the kinetics of the corrosion reactions can be limited. Additionally, for further degradation to take place additional reactants must come in contact with unreacted metal. Along with the polymer network structure, corrosion products can act to further slow transport of corrosive reactants to the substrate. Alkaline conditions at cathodic reaction sites add to the degradation of barrier properties, as the basic local environments cause decreased adhesion and delamination at the substrate-coating interface. As barrier properties decay, the impedance decreases by many orders of magnitude to the point where the film' protective properties are little more influence than the barrier formed by a natural oxide layer at the metal surface. At sufficiently low

impedance it is sometimes possible to observe a second time constant in the low frequency range. This phenomenon is due to the presence of a molecular monolayer of water molecules at the interface between the metal surface and bulk electrolyte. Although small, the charge transfer resistance and double layer capacitance are noticeable in some results. Results from the two model coat systems, PHMC and PTMC, are shown in Figure 1.9. Tests were run at intervals between those shown, but only data sets with significant changes are displayed.

With increasing time in exposure we see two very different performance variations. After 4000 hours of constant immersion in 5% NaCl, the PTMC system maintains largely capacitive behavior. Diffusion of electrolyte into the film steadily increases as phase angle approaches -45°, but no measureable current is able to flow through the system. Impedance values decreases slightly due to diffusion of water into the film, but the magnitudes remain sufficiently high for the coatings to provide barrier protection to the metal.

Results from PHMC measurements are very different. Initially, and after 1000 hours of immersion, the films remain largely capacitive with some signs of electrolyte diffusion, evidenced by ϕ at or below -45°. Impedance at 1500 hours of immersion begins to show resistive behavior, as ϕ approaches 0°. By 2500 hours resistive behavior becomes significant and impedance decreases from . The last curves shown represent the results from 4000 hours immersion. Although still higher than an uncoated substrate, impedance has further decreased and a second time constant is observed at low frequencies. The barrier protection initially afforded by the PPMC film has diminished substantially. The differences in mechanical behavior and film structure correlate with the results obtained by EIS measurements. With a higher storage modulus and crosslink density, the polyester-TGIC films exhibited high barrier protection when exposed to electrolyte. Initial performance of both PHMC and PTMC were comparable, but with increased exposure time, the HAA-crosslinked system showed a significant decrease in protective abilities while the TGIC system maintained its initial performance levels.

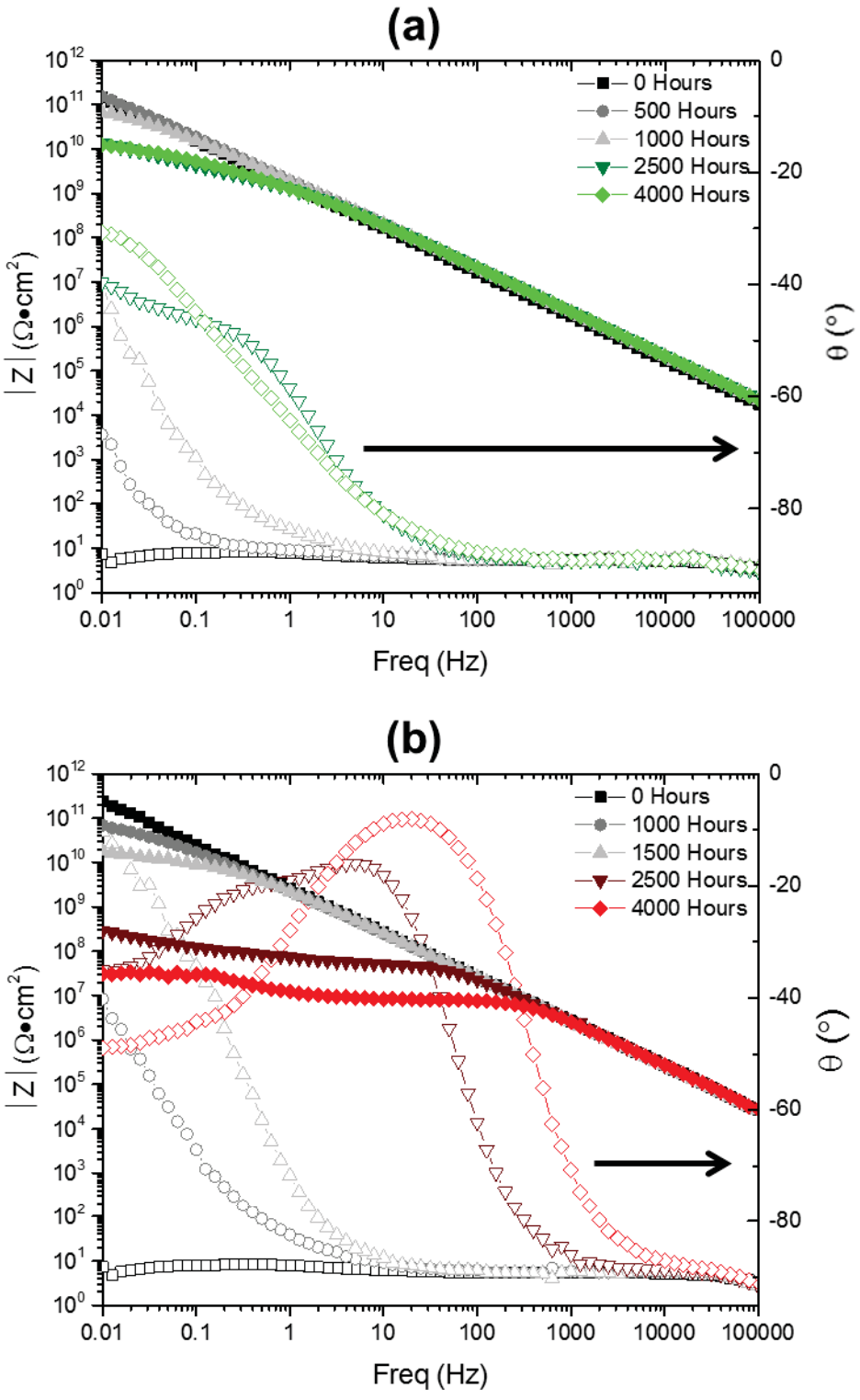

Figure 1.9. Bode impedance and phase angle plots for (a) PTMC and (b) PHMC applied films.

Effects of pigments present in the films can be seen with results from PHFF and PTFF, shown in Figure 1.10. The fully formulated TGIC crosslinked system shows results comparable to its model coat counterpart. After 4000 hours of immersion the impedance values decrease slightly as electrolyte penetrates the film. Even at long exposure times the films maintain high barrier protection. Impedance remains near 10^{11} $\Omega \cdot cm^2$, while ϕ has not increased beyond -60°. The presence of pigments in TGIC films shows little effect in terms of resistance to water penetration. The opposite appears true with the pigmented HAA-crosslinked system. Capacitive behavior with electrolyte diffusion is maintained only to 500 hours of immersion in the PHFF system. Rapid degradation of barrier protection occurs between 500 and 1000 hours as impedance decreases by many orders of magnitude. A second time constant is observed around 2500 hours and at the final measurement period impedance has decreased to a range resembling a failed coating. The PHFF system gives an excellent example for the entire degradation process of coatings applied for barrier protection. Initially the film acts as a perfect barrier, allowing no measureable current flow and showing no sign of electrolyte diffusion. At 500 hours of immersion, the system continues to provide a high impedance barrier, but diffusion of electrolyte into the film is observed by the increase in ϕ to -45°. At this point water has diffused into the film, changing the dielectric behavior, but not penetrating the entire film to create a conductive path between substrate and bulk electrolyte. At 1000 hours of immersion conductive pathways have developed, low frequency impedance has decreased, and ϕ reaches 0°. An equivalent circuit model at this stage would have resistive and capacitive elements in parallel. Resistance becomes apparent due to the increasing presence of conductive pathways through the film. Further degradation of the coating is exhibited in results from 2500 hours of constant immersion. In the low frequency range, double-layer capacitance can be observed by a small increase in impedance, indicating the presence of disbonded areas at the substrate-coating interface [45]. By 4000 hours of constant immersion the film has failed. Impedance has decreased to a level consistent with an uncoated substrate, indicating the formation of cracks or holes in blisters formed by cathodic delamination. The substrate is directly exposed to electrolyte and natural corrosion processes can readily occur.

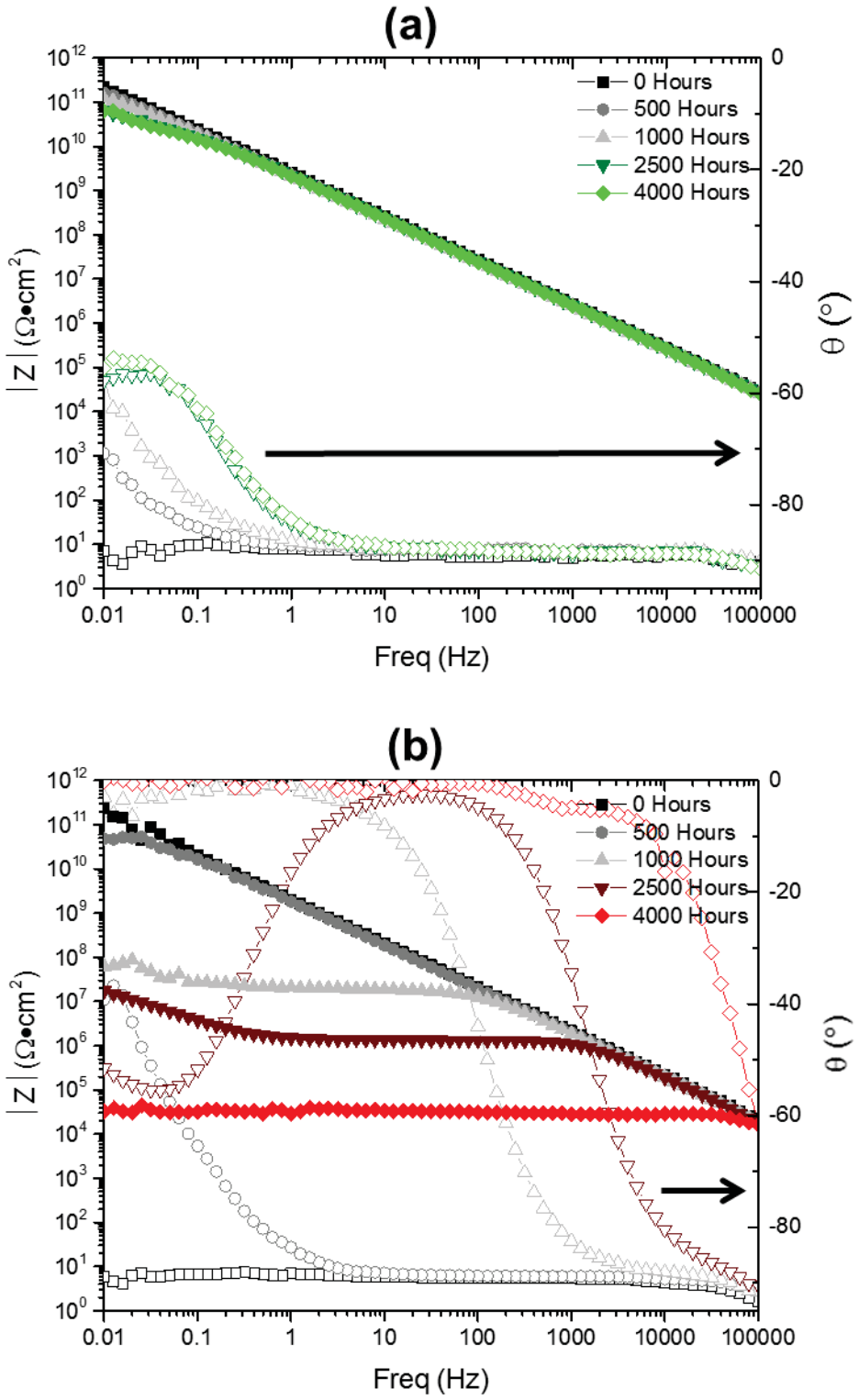

Figure 1.10. Bode impedance and phase angle plots for (a) PTFF and (b) PHFF applied films.

Conclusions

Polyester powder topcoats were investigated for thermal behavior, network properties, and barrier protection to constant immersion in 5% NaCl. Topcoat formulations varied by crosslink chemistry and pigment volume concentration. Formulations based on either TGIC or HAA crosslinking chemistries were prepared as model coatings, free of pigment and extender, or fully formulated coatings with pigment and extender at a concentration of 7.5% by volume. Although both crosslinking chemistries are commonly used in powder topcoat applications, the long term performance of each is very different. Polyesters crosslinked by TGIC hardeners have been long established as superdurable topcoats, but toxicity concerns require the material to be labeled hazardous and use of this chemistry has been restricted.

The crosslinking agents that have been developed to replace TGIC include HAA hardeners. These two chemistries are both similar in terms of application, recommended film thickness, and appearance characteristics, but are very different in terms of barrier protection. Thermal stability of each of the chemistries is very similar. Differences begin to emerge with mechanical testing. The molecular structure of the TGIC molecule is relatively small and limited in segmental motion. This allows cured films crosslinked by TGIC chemistries to develop a higher elastic storage modulus and improved crosslink density.

The HAA molecule is larger relative to TGIC, in addition, the molecular structure includes a carbon chain segment between crosslinkable sites that is capable of molecular motion and chain extension. Initially it was thought water absorption would be higher in the HAA based systems, but gravimetric weight gain experiments showed otherwise. Subject to immersion in water, polyester-HAA free films initially exhibited a steady increase in weight, which plateaued around 1.0% weight gain. After further exposure, the samples exhibited weight loss. Currently, the cause for weight loss in the PHMC and PHFF systems is not fully understood. Water absorption in the TGIC formulations appeared consistent regardless of pigment content.

In terms of electrochemical barrier properties, long-term immersion in 5% NaCl electrolyte proved to further differentiate between the two coating chemistries. TGIC crosslinked coatings showed excellent barrier properties during 4000 hours of constant immersion in 5% NaCl. Through the duration of constant immersion tests, polyester-TGIC coatings maintained capacitive behavior, allowing diffusion of the

electrolyte into the films, but never permitting measurable current flow through the films. Without conductive pathways between the substrate and bulk electrolyte, resistive behavior was not observed, and the aluminum substrate was effectively protected by the barrier properties of the topcoat. Impedance remained over 10^{10} $\Omega \cdot cm^2$, giving insight to why these TGIC crosslinked systems have been such reliable topcoats for outdoor exposure applications. In terms of barrier performance, no distinct difference was observed between pigmented and non-pigmented polyester-TGIC topcoats.

Model polyester-HAA formulations exhibited decreasing performance over immersion time. EIS results from initial immersion measurements showed a low frequency impedance of approximately $2.0x10^{11}$ $\Omega \cdot cm^2$, these values are consistent with initial results from polyester-TGIC systems. Diffusion of electrolyte into the coating was observed while the coating maintained capacitive behavior over short immersion time. An increase in phase angle indicated progressing penetration of electrolyte into the films, and by 1500 hours of constant immersion, conductive pathways were developed between the substrate and bulk electrolyte, represented by resistive behavior in the film. With increased exposure time, a double layer capacitance was observed, indicating active corrosion and cathodic disbondment at the substrate-topcoat interface. Pigmented polyester-HAA topcoats exhibited behavior consistent with their corresponding model coatings, but degradation of the barrier performance of the films occurred more rapidly. The effects of cathodic disbondment were observed at 2500 hours constant immersion. By 4000 hours constant immersion, blisters resulting from delamination had cracked to allow direct exposure of the aluminum substrate to bulk electrolyte.

References

1. McCafferty, E., Introduction to Corrosion Science. Springer: New York, 2010.

2. Tomcsányi, L.; Varga, K.; Bartik, I.; Horányi, H.; Maleczki, E., Electrochemical study of the pitting corrosion of aluminium and its alloys—II. Study of the interaction of chloride ions with a passive film on aluminium and initiation of pitting corrosion. Electrochimica Acta (1989), 34, 855-859.

3. Suter, T.; Alkire, R. C., Microelectrochemical Studies of Pit Initiation at Single Inclusions in Al 2024-T3. Journal of The Electrochemical Society (2001), 148, B36-B42.

4. Guillaumin, V.; Mankowski, G., Localized corrosion of 2024 T351 aluminium alloy in chloride media. Corrosion Science (1998), 41, 421-438.

5. Blanc, C.; Lavelle, B.; Mankowski, G., The role of precipitates enriched with copper on the susceptibility to pitting corrosion of the 2024 aluminium alloy. Corrosion Science (1997), 39, 495-510.

6. de Wit, J. H. W.; van der Weijde, D. H.; Ferrari, G., Organic Coatings. CRC Press: Boca Raton, 2002.

7. Ritter, J. J.; Rodriguez, M. J., CORROSION PHENOMENA FOR IRON COVERED WITH A CELLULOSE NITRATE COATING. Corrosion (1982), 38, 223-226.

8. National Volatile Organic Compound Emission Standards for Consumer Products. In 40 CFR Parts 9 and 59, Agency, E. P., Ed. 1998; Vol. RIN 2060–AF62.

9. Barletta, M.; Lusvarghi, L.; Mantini, F. P.; Rubino, G., Epoxy-based thermosetting powder coatings: Surface appearance, scratch adhesion and wear resistance. Surface and Coatings Technology (2007), 201, 7479-7504.

10. Farrell, R.; Nobel, A., Powder coatings. Metal Finishing (2010), 108, 100-107.

11. Zhou, Z.; Xu, W.; Fan, J.; Ren, F.; Xu, C., Synthesis and characterization of carboxyl group-containing acrylic resin for powder coatings. Progress in Organic Coatings (2008), 62, 179-182.

12. Okadaa, K.; Yamaguchi, K.; Takeda, H., Acrylic/polyester hybrid powder coating system having excellent weather durability. Progress in Organic Coatings (1998), 34, 169-174.

13. GMA acrylics in powder coatings. Focus on Powder Coatings (2003), 2003, 3-4.

14. Bowden, C.; Ostrander, D.; Miller, S. M., Advances in high-performance powder coatings for automotive exterior trim. Metal Finishing (1999), 97, 14.

15. Pilch-Pitera, B., Polyurethane powder coatings containing polysiloxane. Progress in Organic Coatings (2014), 77, 1653-1662.

16. Spyrou, E.; Metternich, H. J.; Franke, R., Isophorone diisocyanate in blocking agent free polyurethane powder coating hardeners: analysis, selectivity, quantumchemical calculations. Progress in Organic Coatings (2003), 48, 201-206.

17. Raju, K. V. S. N.; Chattopadhyay, D. K., 9 - Polyester coatings for corrosion protection. In High-Performance Organic Coatings, Khanna, A. S., Ed. Woodhead Publishing: 2008; pp 165-200.

18. Roman, F.; Montserrat, S., Thermal and dielectric properties of powder coatings based on carboxylated polyester and β-hydroxyalkylamide. Progress in Organic Coatings (2006), 56, 311-318.

19. Gheno, G.; Ganzerla, R.; Bortoluzzi, M.; Paganica, R., Determination of degradation kinetics of two polyester thermosetting powder coatings using TGA and colorimetric analysis. Progress in Organic Coatings (2015), 78, 239-243.

20. Fu, D., Processing of porcelain enamel glass powders for electrostatic spraying. Powder Technology (1995), 85, 65-69.

21. Misev, T. A.; van der Linde, R., Powder coatings technology: new developments at the turn of the century. Progress in Organic Coatings (1998), 34, 160-168.

22. van der Linde, R.; Belder, E. G.; Perera, D. Y., Effect of physical aging and thermal stress on the behavior of polyester/TGIC powder coatings. Progress in Organic Coatings (2000), 40, 215-224.

23. Willcocks, D.; Onyon, L.; Jenkins, C.; Diver, B. Concise International Chemical Assessment Document 8-Triglycidyl Isocyanurate; World Health Organization: 1998.

24. Subramanian, R., Typical ingredients of weather-resistant powder coatings. Metal Finishing (2003), 101, 21-25.

25. Maetens, D., Weathering degradation mechanism in polyester powder coatings. Progress in Organic Coatings (2007), 58, 172-179.

26. Montserrat, S.; Calventus, Y.; Hutchinson, J. M., Physical aging of thermosetting powder coatings. Progress in Organic Coatings (2006), 55, 35-42.

27. Madbouly, S. A.; Serag Eldin, A. F.; Mansour, A. A., Effect of curing on the broadband dielectric spectroscopy of powder coating. European Polymer Journal (2007), 43, 2462-2470.

28. Ramis, X.; Cadenato, A.; Morancho, J. M.; Salla, J. M., Curing of a thermosetting powder coating by means of DMTA, TMA and DSC. Polymer (2003), 44, 2067-2079.

29. Ramis, X.; Calventus, Y.; Cadenato, A.; Roman, F.; Morancho, J. M.; Colomer, P.; Salla, J. M.; Montserrat, S., Mechanical, dielectric and enthalpic relaxation of a thermosetting powder coating based on carboxyl-terminated polyester and triglycidylisocyanurate. Progress in Organic Coatings (2004), 51, 139-144.

30. Belder, E. G.; Rutten, H. J. J.; Perera, D. Y., Cure characterization of powder coatings. Progress in Organic Coatings (2001), 42, 142-149.

31. Mafi, R.; Mirabedini, S. M.; Attar, M. M.; Moradian, S., Cure characterization of epoxy and polyester clear powder coatings using Differential Scanning Calorimetry (DSC) and Dynamic Mechanical Thermal Analysis (DMTA). Progress in Organic Coatings (2005), 54, 164-169.

32. Mafi, R.; Mirabedini, S. M.; Naderi, R.; Attar, M. M., Effect of curing characterization on the corrosion performance of polyester and polyester/epoxy powder coatings. Corrosion Science (2008), 50, 3280-3286.

33. Yang, X. F.; Vang, C.; Tallman, D. E.; Bierwagen, G. P.; Croll, S. G.; Rohlik, S., Weathering degradation of a polyurethane coating. Polymer Degradation and Stability (2001), 74, 341-351.

34. Carter III, R. O.; Paputa Peck, M. C.; Bauer, D. R., The characterization of polymer surfaces by photoacoustic fourier transform infrared spectroscopy. Polymer Degradation and Stability (1989), 23, 121-134.

35. Merlatti, C.; Perrin, F. X.; Aragon, E.; Margaillan, A., Natural and artificial weathering characteristics of stabilized acrylic–urethane paints. Polymer Degradation and Stability (2008), 93, 896-903.

36. Mori, Y.; Honda, T.; Lu, R.; Hayakawa, N.; Miyakoshi, T., Ultraviolet degradation of poly(vinyl alcohol) used in restoration of historical and cultural properties. Polymer Degradation and Stability (2015), 114, 30-36.

37. Gardelle, B.; Duquesne, S.; Vu, C.; Bourbigot, S., Thermal degradation and fire performance of polysilazane-based coatings. Thermochimica Acta (2011), 519, 28-37.

38. Gerlock, J. L.; Bauer, D. R.; Briggs, L. M.; Dickie, R. A., A rapid method of predicting coating durability using electron spin resonance. Journal of Coatings Technology (1985), 57, 37-45.

39. Gerlock, J. L.; Prater, T. J.; Kaberline, S. L.; deVries, J. E., Assessment of photooxidation in multi-layer coating systems by time-of-flight secondary ion mass spectrometry. Polymer Degradation and Stability (1995), 47, 405-411.

40. Bauer, D. R.; Gerlock, J. L.; Dickie, R. A., Rapid, reliable tests of clearcoat weatherability: a proposed protocol. Progress in Organic Coatings (1987), 15, 209-221.

41. Bauer, D. R.; Gerlock, J. L.; Mielewski, D. F., Photostabilization and photodegradation in organic coatings containing a hindered amine light stabilizer. Part VII. HALS effectiveness in acrylic melamine coatings having different free radical formation rates. Polymer Degradation and Stability (1992), 36, 9-15.

42. Gedan-Smolka, M.; Lehmann, D.; Çetin, S., Basic investigations for development of new curing mechanisms for powder coatings. Progress in Organic Coatings (1998), 33, 177-185.

43. Morancho, J. M.; Salla, J. M.; Ramis, X.; Cadenato, A., Comparative study of the degradation kinetics of three powder thermoset coatings. Thermochimica Acta (2004), 419, 181-187.

44. Hill, L. W.; Korzeniowski, H. M.; Ojunga-Andrew, M.; Wilson, R. C., Accelerated clearcoat weathering studied by dynamic mechanical analysis. Progress in Organic Coatings (1994), 24, 147-173.

45. Amirudin, A.; Thieny, D., Application of electrochemical impedance spectroscopy to study the degradation of polymer-coated metals. Progress in Organic Coatings (1995), 26, 1-28.

46. Tahmassebi, N.; Moradian, S.; Mirabedini, S. M., Evaluation of the weathering performance of basecoat/clearcoat automotive paint systems by electrochemical properties measurements. Progress in Organic Coatings (2005), 54, 384-389.

47. Mirabedini, S. M.; Thompson, G. E.; Moradian, S.; Scantlebury, J. D., Corrosion performance of powder coated aluminium using EIS. Progress in Organic Coatings (2003), 46, 112-120.

48. Naderi, R.; Attar, M. M.; Moayed, M. H., EIS examination of mill scale on mild steel with polyester–epoxy powder coating. Progress in Organic Coatings (2004), 50, 162-165.

49. Guth, E., Theory of Filler Reinforcement. Journal of Applied Physics (1945), 16, 20-25.

50. Perera, D. Y., Effect of pigmentation on organic coating characteristics. Progress in Organic Coatings (2004), 50, 247-262.

51. Theocaris, P. S.; Spatis, G. D., GLASS-TRANSITION BEHAVIOR OF PARTICLE COMPOSITES MODELED ON THE CONCEPT OF INTERPHASE. Journal of Applied Polymer Science (1982), 27, 3019-3025.

CHAPTER 2. APPLICATION OF POLYESTER POWDER TOPCOATS TO MAGNESIUM-RICH PRIMERS FOR CORROSION PROTECTION OF ALUMINUM ALLOYS

Abstract

The compatibility of Mg-rich primers (MgRP) and polyester powder coatings was explored with the goal of creating a dual coat system for corrosion protection of aluminum alloys. MgRP's were prepared at various pigment volume concentrations (PVC) and applied to AA-2024-T3. After the primer had cured, the samples were topcoated with polyester-HAA powder coatings, and the resulting systems were investigated for compatibility. Topcoats were applied to the primer by electrostatic spray of the powder coatings. The most effective method of topcoat application was performed by application of the topcoat to substrates preheated to the powder coat cure temperature. When examined by scanning electron microscopy (SEM) the resulting coating systems exhibited no voids in the topcoat film, while the primer-topcoat interface appeared continuous. The dual coat system exhibited three mechanisms of corrosion protection of the aluminum substrate. Initially, the powder topcoat was capable of providing barrier protection for the underlying primer and aluminum substrate. Upon failure of the topcoat, the MgRP exhibited cathodic protection and a secondary barrier effect with increased exposure time.

Introduction

A variety of aluminum alloys have been used in the aerospace industry for decades and more recently growing interest has focused on their use in ground vehicle applications. These alloys can be used in components requiring high mechanical strength while being lighter in weight than their steel counterparts. Issues with aluminum arise when considering the potential for material decomposition by corrosion of the metal. Traditionally the leading compounds in corrosion inhibition of aluminum alloys relies on the use of hexavalent chromium based inhibitors [1]. Recent findings concerning health and environmental impact of chromium compounds have caused increased restrictions and regulation of the chemicals containing chromium [2]. A large volume of research has gone into finding a suitable replacement for chromium, but many state-of-the-art nonchromated corrosion inhibiting systems fall short in providing required performance standards [3]. Many of these new corrosion inhibiting primers still rely on a chromate conversion coating to meet minimum requirements.

In 2004, Nanna and Bierwagen provided proof of concept for a new corrosion inhibiting system that was entirely chromate-free [4]. These new primers, based simply on magnesium particles dispersed in a polymer matrix, were proven to meet and exceed performance requirements for the protection of aluminum in exposure environments. Mg-rich primers (MgRP) utilize the protective phenomenon of sacrificial corrosion or cathodic polarization of the aluminum metal, which is in analog to the well-established protective effect seen in using zinc to protect steel [5-6]. Cathodic protection is provided by coupling dissimilar metals, which causes the more active metal to behave as an anode and preferentially corrode, while the less active metal behaves as a cathode and remains uncorroded. However, zinc is a less active metal ($E_{Zn^{2+}}$=-0.76 V vs. SCE) than aluminum ($E_{Al^{3+}}$=-1.66 V vs SCE), while magnesium is more active ($E_{Mg^{2+}}$=-2.37 V vs SCE) in the galvanic series. When magnesium and aluminum are coupled, the resulting mixed voltage potential is more negative than the corrosion potential of aluminum. The decreased corrosion potential creates a system that is not thermodynamically favorable for oxidation of aluminum and results in cathodic behavior at exposed aluminum sites [7].

Over the last ten years, research has elucidated more details on the protective properties of MgRP by electrochemical characterization techniques including open circuit potential [4, 8-10], electrochemical impedance spectroscopy [8-11], potentiodynamic scanning [8-9, 12], scanning vibrating electrode technique [7, 11], scanning electrochemical microscopy [7, 11], and embedded sensors technology [13-14]. These primers have been shown to exhibit two separate protective effects when applied to aluminum substrates. In the presence of a film defect, with aluminum exposed, the magnesium particles become active anodic sites, forcing cathodic polarization at regions with exposed aluminum. While magnesium is consumed, reactions at aluminum sites are limited to the reduction of water and oxygen, leaving the aluminum metal largely unaffected by exposure. The second protective effect of MgRP is the production of alkaline conditions due to reduction reactions occurring at aluminum surfaces, along with magnesium ions produced by oxidation. Reduction reactions create localized alkaline conditions, which can cause precipitation of magnesium oxide products from the bulk solution [8, 12]. The precipitated magnesium oxide products form a porous layer at the substrate surface which can reduce corrosion by a barrier mechanism. In addition to unfavorable thermodynamic conditions for aluminum

oxidation, results from potentiodynamic scans have showed a decrease in current flow in the coupled systems, indicating restricted reaction kinetics [9, 15].

Primers that rely on cathodic protection by the sacrificial consumption of magnesium are simple in formulation in that they require little more than magnesium powder combined with a polymer binder system. One critical aspect to efficient protection is the pigment volume concentration (PVC) of the particulate magnesium. Primer formulations near critical pigment volume concentration (CPVC) have been shown to display optimum performance characteristics [16-17]. CPVC is a physical state of the composite where particle concentration is at a maximum while binder volume is still sufficient to fill all voids between particles. In this state, theoretically, each particle is in contact with all adjacent particles. Below the CPVC, particle or particle groups can be isolated from contact with adjacent particles. In MgRP, isolated particle groups would be ineffective for cathodic protection due to lack of contact or coupling with the aluminum substrate. While above CPVC, binder content is insufficient for providing a complete adsorbed layer on particle surfaces and filling all interstitial voids between particles.

When formulated near CPVC, all particles in the MgRP are, at least theoretically, fully encapsulated in the polymer matrix while maintaining contact with adjacent particles. In this state, bulk film behavior should mirror threshold limits of electrical percolation theory of particulate composites, where electrical conductivity of disordered media dictates the overall conductivity of the film [18]. Below the percolation threshold, electrical behavior would be dictated by dielectric of the polymer binder. This effect is not singular to metal particles, and has been proven with other particles including carbon nanotubes and other conductive media [19-20]. Optimum MgRP formulation has been demonstrated at pigment concentrations between percolation threshold and CPVC values. In MgRP above the percolation threshold, conductivity between magnesium particles allows the primer film to maintain a coupled state with the metal substrate. Particle concentrations at or slightly below CPVC allows full encapsulation of the magnesium particles by polymer binder, which can decrease the rate of magnesium consumption in primer films [8].

Similar to the push for chromate-free formulations, recent interest in coatings technology has focused on the reduction in VOC emissions by creating solvent-free coatings. One technology area that is rapidly gaining popularity as a high performance, economical, and environmentally friendly technique is

the application of organic coatings in the form of powder coatings [21], especially in topcoats. As they are based on raw materials in solid state at room temperature, powder coatings do not produce wet residuals during manufacturing or application processes. Traditional solvents are not required for film formation, which occurs in a molten state at elevated temperature. Additionally, one intriguing aspect to creating a corrosion protection system which combines MgRP with powder coat topcoats, is the electrostatic spray powder application technique.

Application of powder coatings by electrostatic spray relies on an induced electric field between spray gun and a grounded component to be coated. Paint particles are charged as they pass through the spray gun, and attracted to the grounded part. Paint particle charge improves the guiding effect of the electric field, and provides a means of adhesion of the dry particles to the substrate surface. Coated components are then placed in an oven for curing. Electrostatic spray deposition favors a conductive substrate surface, which is provided by MgRP.

Combining MgRP with powder topcoats has the potential to provide corrosion protection by three mechanisms. Initially the topcoat would provide barrier protection to the substrate, reducing electrolyte diffusion and restricting current flow between substrate and bulk electrolyte. Secondary protection would be provided by the MgRP. In the event of topcoat degradation or physical damage, the primer would initially provide cathodic protection to the aluminum substrate. Further exposure would allow precipitation of magnesium oxides at sites of exposed magnesium and building an oxide layer to provide barrier protection at the defect.

For effective performance of the combined system described above, it is imperative that both MgRP and powder topcoats provide the protective properties displayed by each system independently. Combining these protection systems then relies on the compatibility in application, film formation, and resulting physical structures of each coating layer. At this time it is unclear if any other attempts have been made by other research groups to combine metal rich primers with powder topcoats. Some successful studies have been performed using other corrosion inhibiting primers, in both one coat and two coat powder applications [22-23]. With system compatibility in mind, the research presented below was performed to verify the feasibility of three different stages in combining MgRP with powder topcoats. First, the thermal stability of MgRP formulations at temperatures required for powder topcoat cure must

be verified. Second, the actual application of powder topcoats to MgRPs and resulting topcoat film formation must be free of inherent defects. Finally, the three possible corrosion protection mechanisms must be maintained when the two systems are combined.

Experimental

Sample Preparation

Test panels of aluminum alloy 2024-T3 were prepared by sandblasting with 80 μm alumina grit and degreased with hexanes. MgRP's were prepared at 45% and 50% PVC of magnesium particles. Epon 828 and Epikure 3164 resins were mixed at a 1:1 ratio of equivalent functional groups. BYK 346 was added at approximately 0.5% by weight. Primer batches were diluted with xylenes to achieve low viscosity dispersions for spray application. MgRP was applied by spraying onto cleaned panels at room temperature and allowed to cure for one week before further processing or testing. Final dry film thickness was approximately 90±10 μm as determined by a Positector 6000 under non-ferrous conditions.

Thermogravimetric Analysis (TGA)

Thermal decomposition of the MgRP's was investigated by TGA using a TA Instruments Q500. Samples were prepared by adding approximately 10 mg of cured MgRP to a 100 μL platinum pan. Experiments were performed from room temperature to 800ºC at 20ºC/min ramp rate and under nitrogen gas purge at 50 mL/min. Decomposition Temperature (T_d) was determined at 5% weight loss of the sample.

Powder Coat Application

Application of polyester powder topcoats to MgRP-coated aluminum panels was investigated by electrostatic spray deposition of topcoats to room temperature and preheated MgRP coated panels. The powder formulation used for initial application trials was the PHFF topcoat used in Chapter 1. A Nordson Versa-Spray II electrostatic spray system was used to spray polyester powder topcoats. Powder was allowed 30 minutes of fluidization in the powder hopper before any spraying took place. Panels were sprayed one at a time while suspended by metal hangers in a 12"Hx12"Wx9"D steel faraday cage grounded to the electrostatic spray unit. Air pressures and electrical settings for the Nordson spray unit were 12 psi for the fluidizing air, 15 psi for the powder supply air, 10 psi for the atomization air, and an 80

kV applied voltage potential. Overspray was drawn out of the spray box and collected by a shop-vac fitted with fine particle filters.

Microscopy Techniques

Cross sectional microscopy was performed by a JEOL JSM-6490LV scanning electron microscope (SEM). Samples were prepared by cutting 2 cm x 2 cm square sections from prepared panels, and casting the samples in EpoFix epoxy casting resin. Upon hardeneing, the samples were polished on a Struers TegraPol-25 with a variety of polishing disks. Fully polished samples were finished with an MD-Nap disk and DiaPro 1 µm water based diamond suspension. Polished samples were coated with a thin film of carbon for proper grounding and imaging in the SEM unit.

Optical surface profilometry (OSP) was performed using a PAR Scanning Electrochemical Workstation M370 outfitted with a Keyence LK-G32 sensor head laser. Sample surfaces were mapped over an area of 3000 µm x 3000 µm, with measurements taken at 10 µm/point, and a scan speed of 1000 µm/s. The software package, M370 Version 4.05.1967 PAR, was used to calculate surface roughness average (S_a) by

$$S_a = \frac{1}{MN}\sum_{j=1}^{N}\sum_{i=1}^{M}\left[\eta\left(x_i, y_j\right)\right] \quad \text{(Eq. 2.1)}$$

and root mean square roughness (S_q) by

$$S_q = \sqrt{\frac{1}{MN}\sum_{j=1}^{N}\sum_{i=1}^{M}\left[\eta^2\left(x_i, y_j\right)\right]} \quad \text{(Eq. 2.2)}$$

where η is the height measurement at (x,y) and the product MN is the number of total data points.

Electrochemical Measurements

Characterization of electrochemical behavior was performed using a Gamry Reference 600 Potentiostat with Gamry Framework Version 6.20/EIS300 data acquisition software. Open Circuit Potential (OCP) was performed to monitor the active corrosion potential of the exposed systems. Bare metal samples of aluminum or magnesium were tested in an 80 mL beaker acting as an electrochemical cell. The metal strips 5mm x 50mm were immersed in 5% NaCl electrolyte with a platinum mesh counter electrode and SCE reference. Electrochemical cells for bare MgRP and topcoated MgRP samples consisted of a glass cell clamped to the sample with an o-ring sealing the connection from leakage. Long term OCP measurements (>1 Hour) were performed at 20 second intervals with voltage stability set to 0

mV/s. Electrochemical impedance spectroscopy (EIS) was performed to monitor impedance of topcoated MgRP systems with and without artificial defects in the coating. Defects were created using a 1 mm drill bit to penetrate the protective coatings and expose the metal substrate. A glass electrochemical cell and o-ring assembly were clamped to the sample with the artificial defect centered in the cylinder. The substrate was connected as the working electrode while a platinum mesh was the counter electrode and a saturated calomel reference electrode (SCE) was used as a reference electrode. Electrolyte solution was prepared as a 5% NaCl solution using 18 MΩ ultra-pure water. Total exposed area of the working electrode was 7.06 cm^3. Measurements were taken over a frequency range of 100,000-0.01 Hz with 10 collection points per frequency decade. An AC potential perturbation was applied at 10 mV RMS versus open circuit potential. Samples remained in constant immersion with tests performed at daily intervals. Constant immersion samples were left uncovered at room temperature. Solution levels were monitored and, under the assumption that no salts would evaporate from the solutions, electrolyte levels were maintained by adding DI water until the original fill volume was achieved. At two week intervals the electrolyte solutions were drained and replaced by fresh solution.

Results and Discussion

Application of Powder Topcoats to Mg-Rich Primers

Initial considerations regarding application of powder topcoats over MgRP were focused on feasibility of the combined coating technologies and stability of the MgRP film. In regards to feasibility, the primary concern was the potential for shielding of the electrostatic field by the MgRP layer. In regard to this concern, it is important to understand the roles played by electrostatic effects and charged coating particles. Bulk conductivity, or conductivity between the substrate and primer, is not as important as surface conductivity of the primer. As the coating particles are not wet, they rely on adhesion to the substrate surface by static charges. A number of techniques exist to increase surface activation of a nonconductive material [24-26]. One in particular includes the application of fine copper particles to the substrate surface, increasing surface conductivity [27]. MgRP formulations at or near CPVC have previously been shown to provide excellent protection for aluminum substrates. In these formulations, protection provided by magnesium particles is believed to rely largely on the presence of a conductive pathway between particle and substrate for sacrificial oxidation of the magnesium metal. As supplied, the

particles have a resistivity of 4.5E-8 Ω·m, equivalent to a conductivity of 2.25E7 S·m and is consistent with values for conductive metals. Ultimately it was assumed that the conductivity of MgRP would not hinder electrostatic effects for powder application, and no surface pretreatments were considered for applying powder topcoats to MgRP.

As safety is always a primary concern, thermal stability of the MgRP was the first issue investigated for overall compatibility of the combined coatings systems. Powder coatings require cure cycles at elevated temperatures, often above 200°C. Magnesium is a highly reactive metal, without recently developed processing techniques the stability of particulate magnesium would be questionable. As supplied, the Mg-particles used in this research have a thin oxide layer at the particle surface. In this form, the temperature at which spontaneous combustion occurs is over 500°C, far above recommended cure temperatures for any of the powder topcoats utilized in this research. To determine thermal decomposition of the MgRP, TGA was performed on cured MgRP samples well beyond the recommended powder topcoat cure temperatures. Results from TGA analysis are shown in Figure 2.1. Cure temperatures for both polyester powder topcoat chemistries are also highlighted in the plot. MgRP samples exhibited T_d at approximately 290°C, nearly 100°C higher than recommended cure temperatures for either topcoat. A small weight loss of 1-3% is observed around 180°C, and upon further investigation, was assumed to be due to loss of volatiles from the epoxy binder used in the MgRP formulation. At temperatures below 290°C the primer was considered stable for further application studies. Similar results were observed by Ravindran et al. with when using a glycidyl carbamate resin [28]. Three distinct stages were observed over the temperature ramp; including a low temperature loss of volatiles, random decomposition of polymer chains above 300°C, and an increase in weight at higher temperatures due to the formation of magnesium oxides.

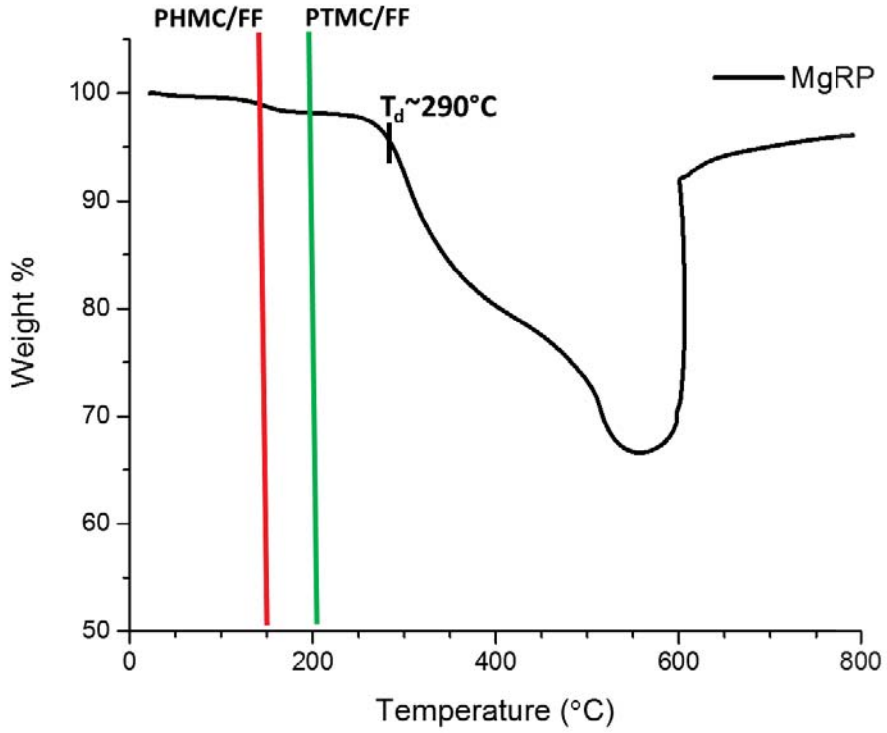

Figure 2.1. Thermogravimetric analysis of the MgRP. Colored bars indicate powder topcoat cure temperatures.

With the goal of characterizing a dual-coat corrosion protection system, the proof of concept in applying powder topcoats to MgRP was fundamental for this research. Thermal stability of MgRP was proven at temperatures far above recommended cure temperatures for all powder formulations selected for investigation. Concerning film conductivity, initial application trials were performed with panels coated by 50% PVC MgRP. At a pigment volume above CPVC the primer film was assumed to have optimum conductivity, allowing maximum electrostatic effects by electrostatic spray of the powder topcoat. Powder topcoats were applied to MgRP coated panels at room temperature and immediately cured by recommended cure schedules for the polyester topcoats. Baseline samples were also prepared by application of the powder topcoats to bare aluminum panels. Air pressures and electrical settings of the electrostatic spray system were not changed between coating application to bare aluminum or MgRP coated aluminum panels.

Images shown below include macroscopic views of the coated panels along with microscopic cross sections. Panels prepared without primer produced cured films with high gloss, smooth finish, and no macroscopic defects in the film, as seen in Figure 2.2. Microscopic analysis of the cross sections shows no inherent defects in the film, and the interface between substrate and topcoat appears continuous. In the absence of primer, the topcoat films form as intended as they melt, flow, and level to create a defect-free film. Initial attempts at applying powder topcoat to MgRP, shown in Figure 2.3, produced very different results compared to the primer-free systems. Obvious film defects were observed at both macroscopic and microscopic scales. Film surfaces were dull, rough, and appeared to have voids trapped beneath the film surface. One positive observation is that the MgRP proved sufficiently conductive to support electrostatic deposition of the powder topcoat. Cross sectional microscopy confirmed the presence of voids throughout the film, specifically in areas with increased irregularity in the MgRP film. Proper film formation was not achieved, resulting in a visibly rough surface finish and inherent defects in the topcoat film.

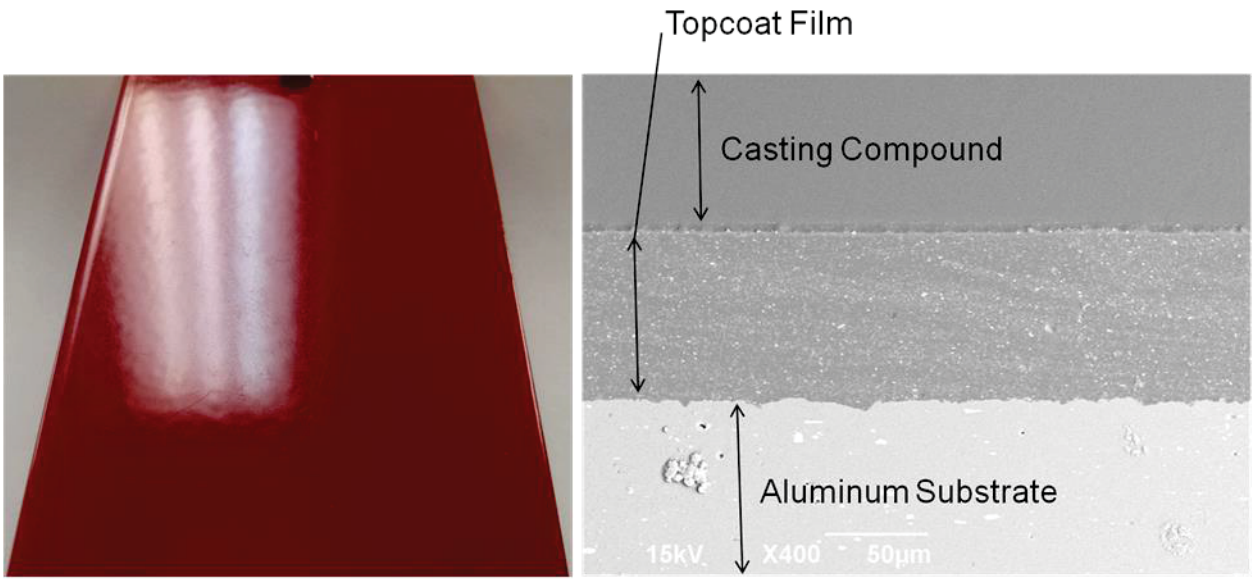

Figure 2.2. Surface finish and cross-sectional view of electrostatic spray topcoat without primer.

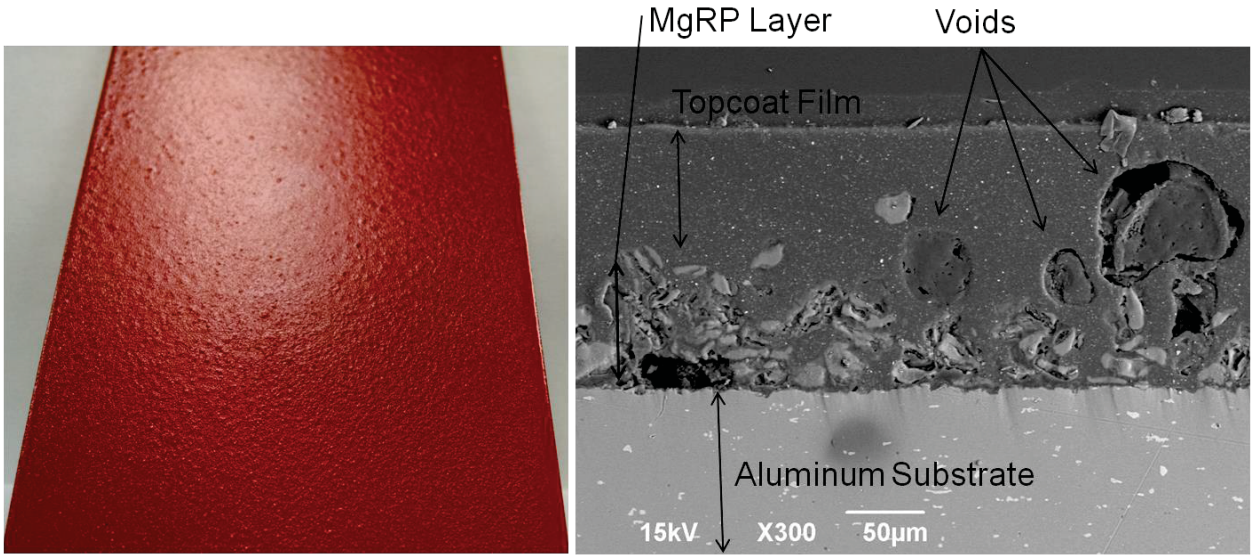

Figure 2.3. Surface finish and cross-sectional view of electrostatic spray topcoat with 50% PVC MgRP.

Though proof of concept was confirmed regarding the feasibility of topcoat application to MgRP by electrostatic spray, there were many flaws in the fully cured system. Powder coat film formation relies on the sequence of particle melt, flow, degassing, and leveling in order to form a uniform film across a substrate surface. One significant difference between panels with and without MgRP is surface topology. Panels were studied by optical surface profilometry (OSP) in order to characterize surface roughness. OSP is a non-contact technique utilizing visible laser light to measure changes in surface profile on the dimensional order of microns. Surface roughness values for sandblasted aluminum, 45% MgRP, and 50% MgRP are listed in Table 2.1. Results from profilomerty measurements are shown in Figure 2.4, which compares a sandblasted aluminum panel to a similar panel coated with 50% PVC MgRP. Roughness average and root mean square roughness of the 50% MgRP coated panel was calculated to be approximately five times greater than that of the sandblasted aluminum panel. It was believed that the large difference in surface profile between panels with or without primer was the key factor in poor film formation with 50% MgRP. High roughness of the primer films formulated above CPVC created a surface topography too irregular for the proper film formation of the topcoats. Additionally, it is possible that the increased roughness caused local variations in the applied electric field similar to the Faraday cage effect [29]. Large flat surfaces are ideal for strong electric fields, while complex shapes can prove difficult to coat. Electrostatic lines become concentrated on sharp edges, creating a resistance to powder deposition

in recesses and inside corners. Poor topcoat film formation on the 50% MgRP could be due to localized shielding effects by topographical peaks in the primer surface, drawing powder away from recesses in the film, and creating a non-uniform deposition profile.

Polyester powder coatings studied in this project were based on commercially available formulations well established in industry and changing the topcoat formulations was to be avoided unless absolutely necessary. Primer formulations, on the other hand, were pigmented epoxy-amide formulations created in lab batches. For further application, testing aluminum panels were coated with a 45% PVC MgRP. Being below CPVC of the magnesium particles, this primer formulation was found to have surface roughness values similar to the sandblasted aluminum surface. This effect is observed in the surface topography shown in Figure 2.5. Electrostatic spray application of powder topcoats was repeated with the 45% PVC MgRP panels, the results from which are shown in Figure 2.6. Under inspection by the naked eye, the topcoat films appeared much smoother than the ones applied on 50% PVC MgRP, but some small surface irregularities were still observed. Analysis of cross sections showed much more uniform topcoat film formation with 45% PVC MgRP than with 50% PVC MgRP. A number of small voids were still observed in the cured topcoat films, indicating some level of incomplete degassing of the coating.

Table 2.1. Calculated surface roughness values for sandblasted Al2024 and each MgRP formulation.

	Sandblasted Al2024	45% PVC MgRP	50% PVC MgRP
Sa (μm)	3.351	6.999	17.78
Sq (μm)	4.066	8.857	22.74

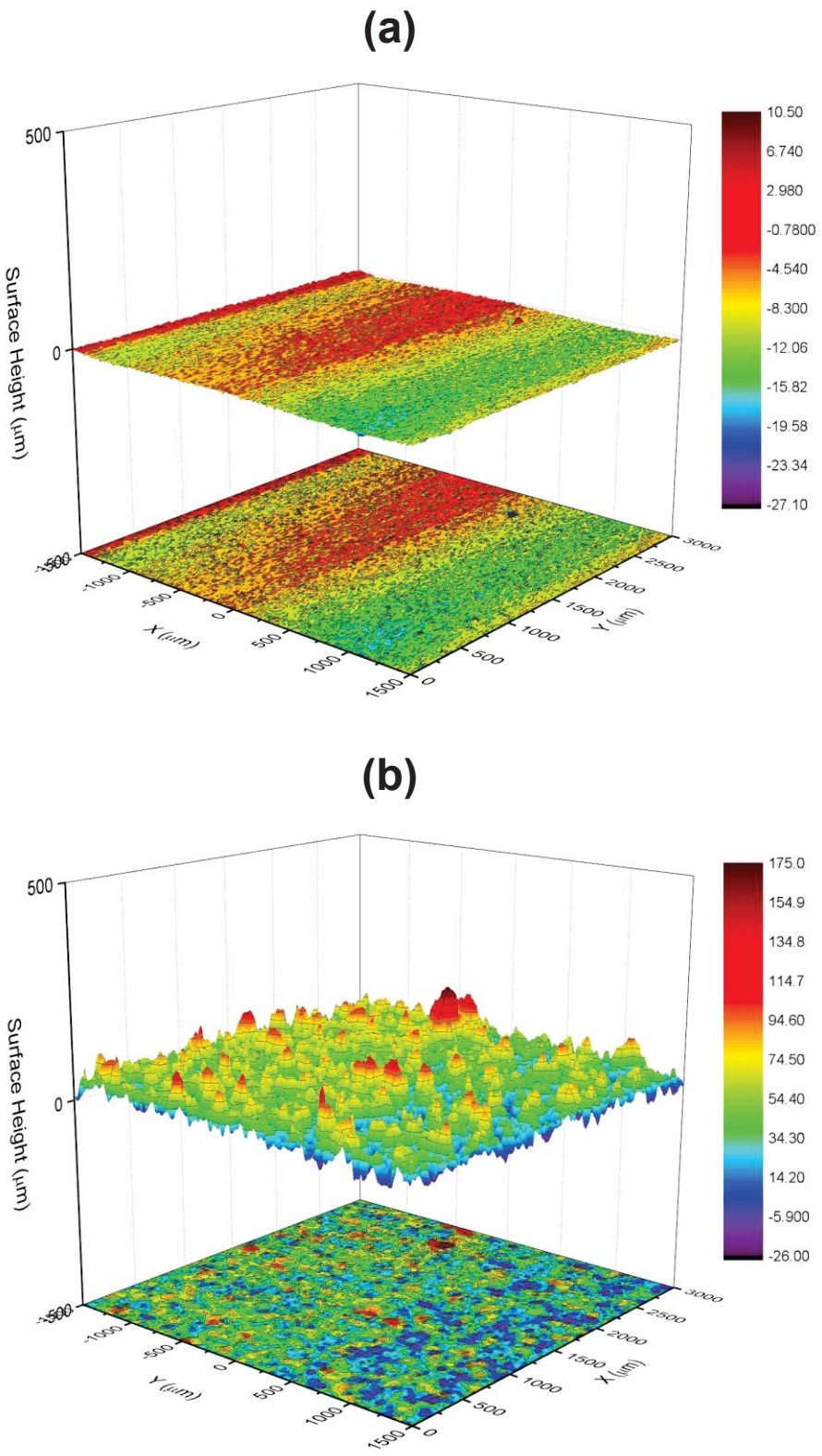

Figure 2.4. Surface profiles of (a) sandblasted aluminum and (b) 50% PVC MgRP.

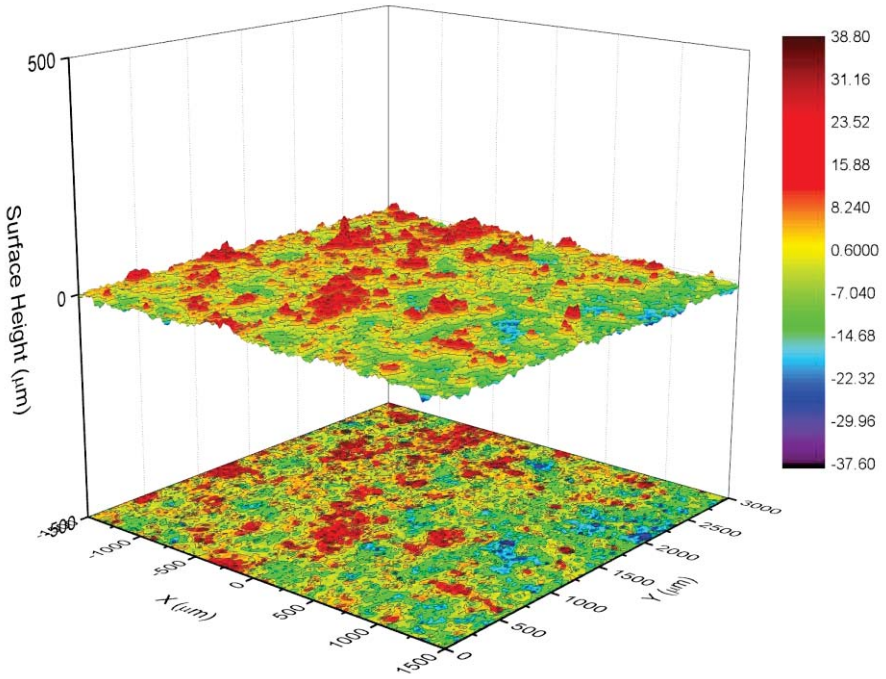

Figure 2.5. Surface profile of 45% PVC MgRP.

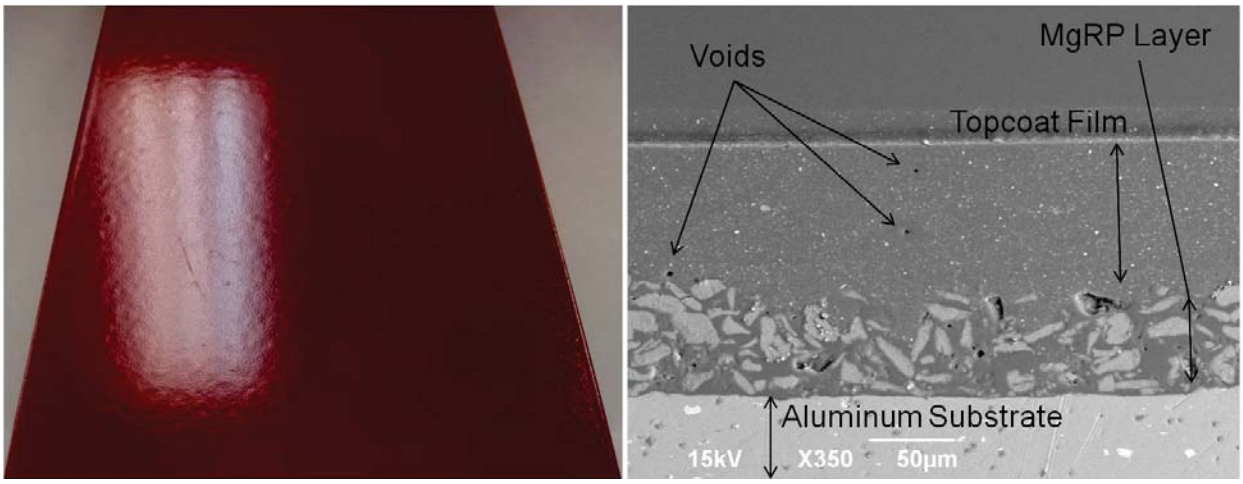

Figure 2.6. Surface finish and cross-sectional view of electrostatic spray topcoat on a room temperature panel with 45% MgRP.

A phenomenon that has not been mentioned up to this point is the potential for adverse interactions between the MgRP and powder topcoat chemistry used in these tests. Crosslinking of carboxylated polyesters and Primid hardeners involves esterification reactions between carboxylic acid groups of the polyesters and hydroxyl groups of the Primid molecules. In addition to molecular crosslinks, a natural byproduct of the reaction is water. Magnesium is a highly active metal and, in the presence of

water, reacts to cause hydrogen evolution. At room temperature the reaction between MgRP and water is rapid enough to see hydrogen bubbles form within the first few seconds of immersion. In this complex system it is difficult to definitively determine the extent of interaction between reactions producing water, interaction between water and magnesium, and resulting hydrogen evolution in a system exposed to temperatures approaching 200°C. What was apparent throughout the topcoat application trails was the formation of inherent defects in the topcoat film when powder was applied to room temperature panels and then cured. For some reason not yet indentified, the topcoat was not properly degassing during curing to form uniform films.

To improve degassing of the topcoat film, a slower film formation technique was required. Previous trials were all performed on room temperature panels, depositing powder particles in a single layer to coalesce into a finished film. The issue with this technique stemmed from the lack of complete degassing, in fact voids were formed due to gas bubbles trapped in the polymer network during curing. One technique for possibly improving degassing of the films involves preheating the panels and spraying when the substrate is still hot. In theory, this would allow a uniform film build and improve the degassing by allowing gradual melt and flow of the powder particles. A singular crosslinked network would be formed as long as total application time is less than the gel time for the coating. An example of panels prepared by this technique, along with cross sectional images, can be seen in Figure 2.7. Panels were preheated at the recommended cure temperature for the topcoat for approximately 30 minutes, and powder topcoat was deposited by electrostatic spray. In order to assure slow particle deposition, pressures for powder supply air and atomization air were decreased to 5 psi and 4 psi respectively. Voltage potential settings were not changed, remaining at 80 kV, and fluidizing air pressure was also unchanged, at 12 psi. After hot spray application and cure cycling, the topcoated samples with 40% MgRP displayed surface characteristics consistent with primer-free panels. The topcoat surface appeared smooth and free of any macroscopic defects. SEM imaging of sample cross sections revealed no inherent defects in the film. The topcoat flowed and filled in all irregularities in the primer surface, ultimately forming a uniform film.

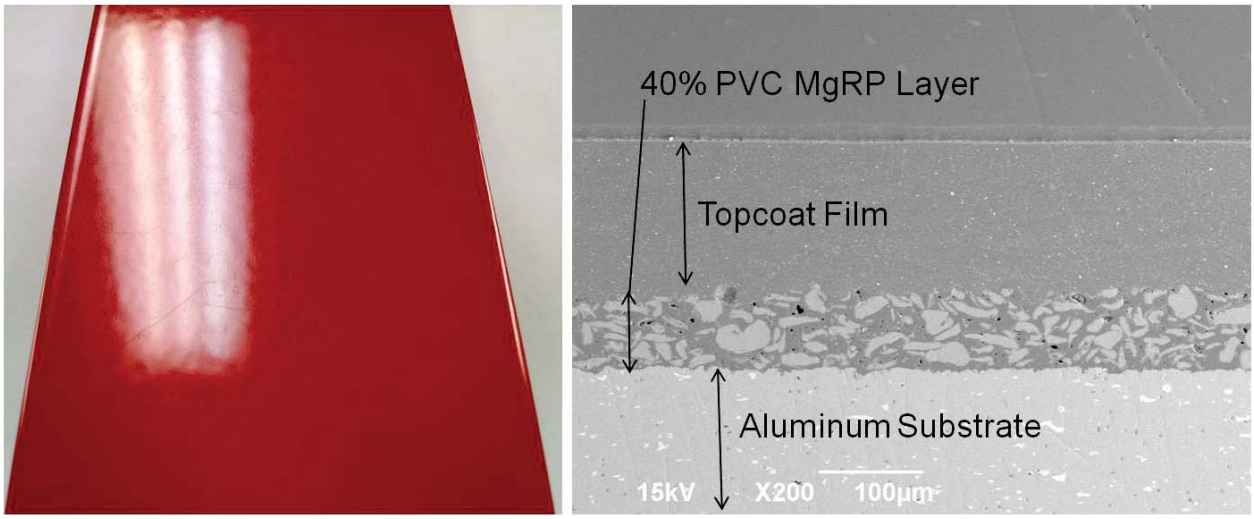

Figure 2.7. Surface finish and cross-sectional view of electrostatic spray topcoat on a preheated panel with 45% MgRP.

Investigation of Barrier Protection by Powder Topcoats Applied to Mg-Rich Primers

Verification of barrier property performance by the topcoat was done by EIS measurements. Results shown in Figure 2.8 below represent the topcoat performance after 1 hour of immersion in 5% NaCl. With phase angle remaining near -90° throughout the frequency scan, and low frequency impedance on the order of 10 GΩ, the initial barrier properties are consistent with the systems measured in Chapter 1 that did not include an MgRP layer.

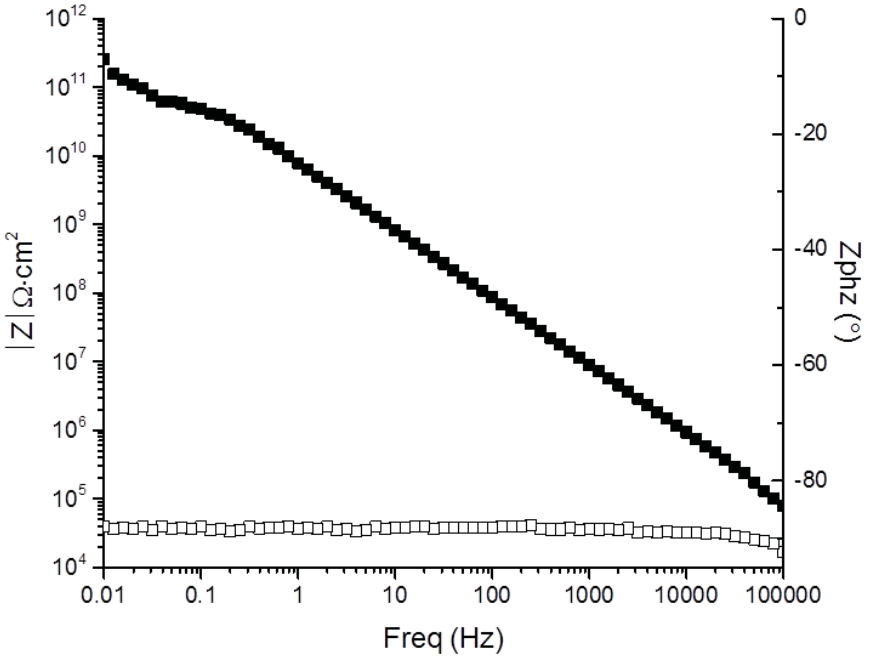

Figure 2.8. EIS results from 1 hour immersion of a topcoated, 40% PVC MgRP, hot spray sample with no artificial defect in the coating.

Cathodic Protection by Mg-Rich Primers

Topcoats applied for barrier protection to electrolyte penetration are limited by the physical state of the films. Complete electrolyte penetration or defect formation is inevitable. Employing a dual-coat system with an active metal-rich primer beneath the topcoat is one potential method for increasing the protective lifetime of powder topcoats. The MgRP used for these studies has already been shown to provide cathodic protection to aluminum alloys in a similar manner as zinc protects steel [4]. With thermal stability of the primers confirmed, and application of powder topcoats proven effective, it was possible to begin electrochemical characterization of the combined systems. Measurement of open circuit potential in electrochemical cells provides a simple means of observing the active corrosion potential of a system. Results in Figure 2.9 show the effect of coupled aluminum and magnesium metals. The corrosion potential of a bare aluminum alloy 2024-T3 is displayed as a solid black line. Under exposure to 5% NaCl, the metal exhibited a voltage potential at approximately -0.600 V vs SCE, which is consistent with the expected potential range for these aluminum alloys. Under similar exposure condition, a bare magnesium sample was measured at -1.600 V vs SCE, shown as a solid gray line. The dashed curve in the plot,

displayed in red, exhibits the effects of MgRP coupled with an aluminum substrate. This data was taken from an Al2024-T3 panel coated with MgRP and polyester powder topcoat. A defect was then created with a small drill bit measuring approximately 1 mm in diameter. Defect depth was sufficient to penetrate both layers of the applied films, leaving a small area of the metal substrate open to exposure.

A glass electrochemical cell was clamped to the sample with the defect centered in the cell. Measurements at immediate stages of electrolyte exposure show the voltage potential of this system to be at -1.200 V vs SCE. As exposure time increases, the potential gradually increases until equilibrating around -0.800 V. The gradual change in potential is due to sacrificial corrosion of Mg-particles in the primer layer. Magnesium consumption shifts the potential of the system towards that of bare aluminum. It is important to note that over the exposure interval shown, measured voltage potential plateaus at level below that of bare AA2024-T3. The system equilibrates at a level more negative than the anodic half-cell reaction of aluminum, effectively showing protection of the Al alloy by inducing cathodic behavior of the aluminum.

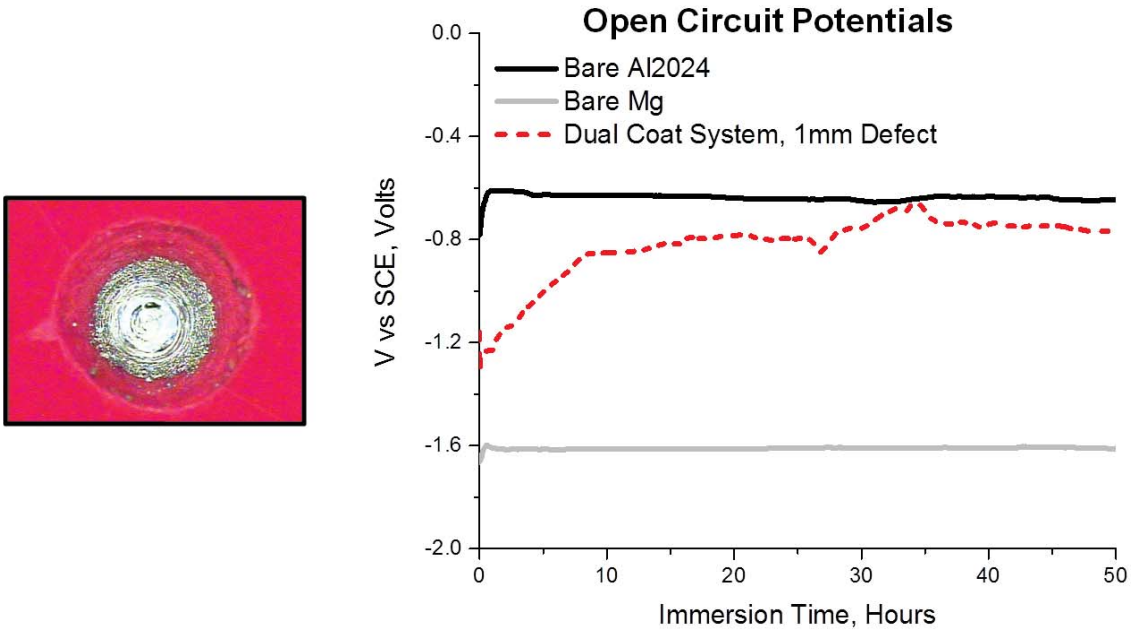

Figure 2.9. A 1 mm artificial defect (left), and OCP results from bare Al2024 (black), bare magnesium (gray), and applied topcoat/40% PVC MgRP on Al2024 with defect (dashed-red).

Time durations for cathodic protection are variable and are closely related to defect size or ratio between surface areas of the exposed metals. Higher magnesium exposure relative to aluminum should provide longer cathodic protection as there is simply more magnesium to be consumed. It has been observed in previous work that the consumption of magnesium is reduced in MgRP when compared to coupled aluminum and magnesium electrodes [8]. Reduced magnesium consumption rates are thought to be due to the particle encapsulation in polymer binder in the primer.

The secondary protective effect provided by sacrificial corrosion of magnesium can be observed with EIS measurements on samples in constant immersion. Results shown in Figure 2.10 include measurements from systems with and without MgRP at 0 hours and 24 hours immersion. Each sample contained an artificial defect, created by a 1 mm drill bit, leaving a small area of the substrate exposed. Impedance curves shown in dark red and red represent results from a coating system without primer at 0 hours and 24 hours immersion respectively. Low frequency impedance is on the order of 1 MΩ, consistent with expected values for an applied topcoat with small defect. After 24 hours exposure the impedance has decreased slightly but remains at a similar order of magnitude. The system including MgRP, shown by black and gray curves, exhibits a very different effect under exposure. Initially the impedance is slightly below that of a bare metal, but after 24 hours immersion (gray curve) is increased two orders of magnitude to approximately 10 MΩ. Increased impedance values indicate a restriction in current flow through the system, ultimately limiting the kinetics of further corrosion reactions. This effect can be explained by the formation of a thin magnesium oxide film in the defect area, similar to observations from previous works [8, 12]. The presence of a precipitate film at the defect site was visible to the naked eye by 24 hours of immersion in solution. Though the oxide layer does not restore barrier protection to a level consistent with that of an undamaged topcoat film, the protection of the substrate is improved considerably when compared to the primer free system.

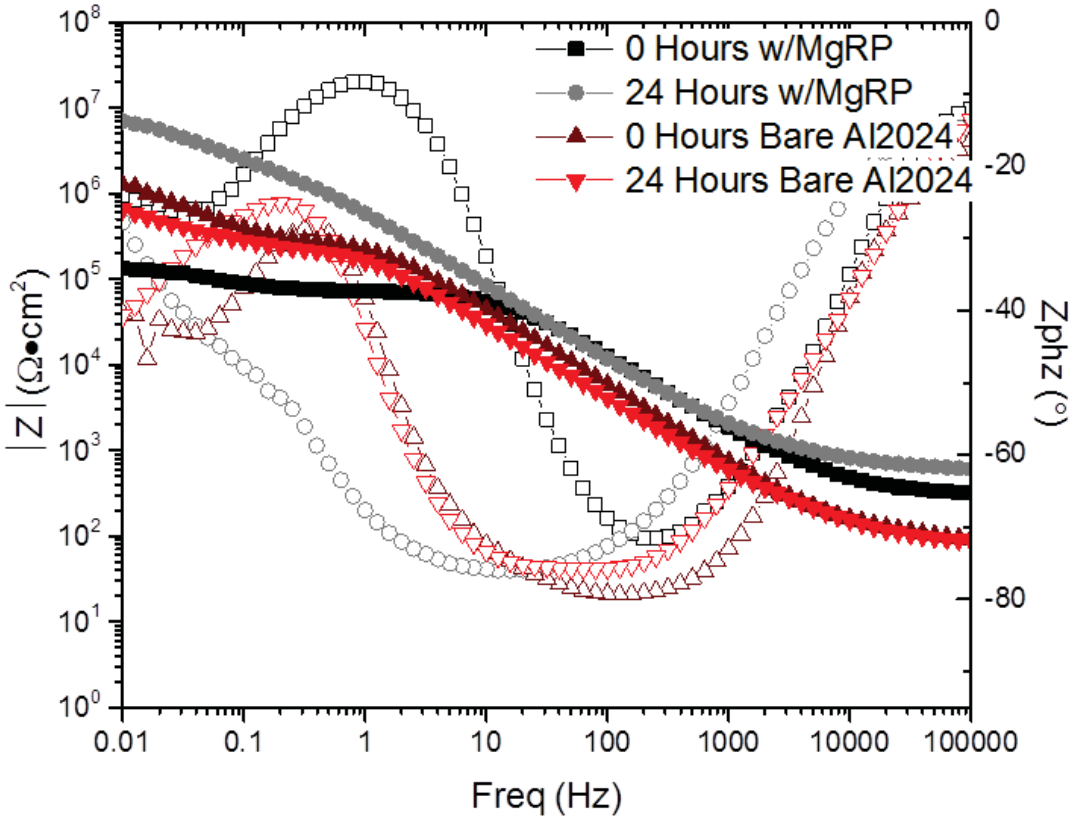

Figure 2.10. EIS results from systems with artificial defect in constant immersion. Data is shown from 0 hours without primer (dark red), 24 hours without primer (red), 0 hours with 40% PVC MgRP (black), and 24 hours with 40% PVC MgRP (gray).

Conclusions

Powder topcoats investigated in the previous chapter were found to retain good barrier protection under constant electrolyte immersion, some achieving >4000 hours exposure without allowing significant current flow through the films. Performance of these systems relies heavily on the physical state of the films. Any film defects, whether inherent or induced, can potentially compromise the barrier effect and render the coating permeable to water and other electrolytes. Additionally, even undamaged films will eventually submit to electrolyte penetration or diffusion, allowing conductive pathways to develop and initiate corrosion reactions at the substrate surface. Utilizing a dual coat system, involving a protective topcoat applied over a metal-rich primer, can potentially increase the protective life of the coating system and the lifetime of the underlying metal structure.

Metal-rich primers, particularly MgRP for aluminum substrates, have been shown to provide cathodic protection to metal substrates. Protective effects depend on coupling of Mg and Al metals. In a coupled system, magnesium is oxidized, effectively inducing cathodic polarization of the less active aluminum metal. The resulting open circuit potential of the system is below that of aluminum and this polarity creates an environment thermodynamically unfavorable for aluminum oxidation. Cathodic polarization requires the magnesium and aluminum metals to be coupled, allowing electron flow between the dissimilar metals. In MgRP, this effect relies on formulation at or near CPVC. Magnesium particles that are not connected to the system create local electrochemical cells and do not contribute to cathodic protection of the substrate. MgRP formulations above the percolation threshold and near CPVC allow conductivity of the Mg-particles to dominate over dielectric of the binder, resulting in a conductive film. An additional effect of sacrificial corrosion of magnesium involves the formation of oxide layers in the defect. Anodic sites produce magnesium ions soluble in water. Reduction reactions at cathodic sites increase local pH values. In these local alkaline environments, magnesium oxides precipitate out of solution to form a porous oxide barrier [8]. Dual coat systems combining MgRP and powder topcoats require compatibility of the two coating systems. Initial concerns about combining these systems revolved around the thermal stability of MgRP at temperatures required for powder topcoat cure. TGA experiments were conducted to determine decomposition temperature of cured MgRP films.

Determined at 5% weight loss, MgRP T_d was found to occur around 290°C, nearly 90°C higher than the highest recommended cure temperature for the powder topcoat chemistries. With thermal stability of the primer confirmed, compatibility concerns turned to the actual application and film formation of powder topcoats to MgRP films. The most common method for powder coat application is electrostatic spray. Powder is atomized by compressed air and forced into an electrostatic field between the spray gun and grounded substrate. The particles become charged and attracted to the substrate. Without proper electrostatic effects, deposition of the powder particles is hindered, creating a system inefficient for coating application. It was originally unknown what kind of effect the MgRP film would have on powder topcoat application. Initial tests were performed by electrostatic spray of room temperature panels coated with 50% PVC MgRP. Topcoat application was proven successful, but additional concerns arose. Comparison of topcoat films applied to panels with and without MgRP showed very different film

formation. Increased roughness and surface irregularities of the MgRP, compared to a sandblasted aluminum surface, hindered the complete degassing of the topcoat. Repeating application trials with 40% MgRP showed significant improvements to topcoat film formation. At 50% PVC for the magnesium particles the primer is above CPVC, which occurs at approximately 45%. Reformulating the primer to 40% PVC allows the system to cure with more resin filling voids between magnesium particles, ultimately decreasing irregularities in the primer surface. Though much improved, topcoat films continued to display surface defects and small voids in cross sections. Continued application trials with 40% PVC MgRP proved successful when the panels were preheated and sprayed while hot. Panels were preheated to recommended cure temperatures of the topcoat, sprayed by electrostatic deposition, and then placed back in the oven to cure. With preheated panels, the powder particles were immediately melted, initiating flow and degassing of the film while powder was still being deposited. Cross sectional microscopy revealed no inherent defects in the topcoat films prepared by this method. The surface finish of topcoats applied to preheated MgRP samples was consistent with the surface finish of coated panels without a primer layer. Initial barrier protection provided by the powder topcoat is consistent with results from systems that did not include a MgRP layer. Cathodic protection of aluminum by MgRP under powder topcoats was investigated by OCP and EIS. Dual coat systems with artificial defects were tested by OCP measurements to monitor voltage potential.

Coupling interactions between magnesium particles embedded in the primer film and aluminum substrate were evidenced by the initial potential of -1.200 V vs SCE. Oxidation of magnesium particles consumes the metal, causing the voltage potential to increase and equilibrate at -0.800 V by 50 hours immersion. Despite magnesium consumption, the system maintains a voltage potential below that of bare aluminum, which was measured to be approximately -0.600 V vs SCE. In terms of corrosion reactions, magnesium is a highly active metal, second only to lithium in the galvanic series. With both magnesium and aluminum exposed at the defect site the more active magnesium metal is oxidized, forcing cathodic polarization and reduction reactions in the area of exposed aluminum, an event termed cathodic protection.

A secondary protective effect was observed with EIS measurements on systems including an artificial defect. Without MgRP, low frequency impedance was consistent with the values expected for a

bare metal. After 24 hours immersion there was no significant change in impedance. Systems incorporating MgRP displayed very different behavior. Immediately after immersion, low frequency impedance mirrored expected values for a bare metal. Repeating the experiment at 24 hours immersion showed an increase in low frequency impedance, indicating restriction of current flow and limiting corrosion kinetics. The impedance increase can be explained by the formation of a MgO layer at sites with exposed aluminum. Reduction reactions at cathodic sites create local regions of high pH. MgO is soluble in water at neutral pH, but precipitates out of solution in alkaline conditions. At exposed aluminum surfaces, precipitates form an oxide layer, and act as a barrier to current flow.

The studies performed for this work have provided insight to creating dual coat corrosion protection systems employing magnesium-rich primers for cathodic protection along with polyester powder topcoats for barrier protection of the Al alloy substrates. Primer formulations were shown to be thermally stable at temperatures required for powder coat curing. Proof of concept in application of powder topcoats to MgRP was provided. When applied by electrostatic spray to preheated MgRP coated panels, the powder topcoat film formation was consistent with films cured to bare aluminum panels. EIS provided further confirmation of topcoat barrier properties, as the impedance of the dual coat systems was measured to be greater than 10^{11} $\Omega \cdot cm^3$, indicating excellent barrier protection. With artificial defects in the film, the MgRP was observed to induce cathodic protection of the aluminum substrate, and provide a secondary barrier protection mechanism by magnesium oxide precipitation at sites of exposed aluminum.

References

1. Clark, W. J.; Ramsey, J. D.; McCreery, R. L.; Frankel, G. S., A Galvanic Corrosion Approach to Investigating Chromate Effects on Aluminum Alloy 2024-T3. *Journal of The Electrochemical Society* (2002), 149, B179-B185.

2. Twite, R. L.; Bierwagen, G. P., Review of alternatives to chromate for corrosion protection of aluminum aerospace alloys. *Progress in Organic Coatings* (1998), 33, 91-100.

3. Osborne, J. H.; Blohowiak, K. Y.; Taylor, S. R.; Hunter, C.; Bierwagon, G.; Carlson, B.; Bernard, D.; Donley, M. S., Testing and evaluation of nonchromated coating systems for aerospace applications. *Progress in Organic Coatings* (2001), 41, 217-225.

4. Nanna, M.; Bierwagen, G., Mg-rich coatings: A new paradigm for Cr-free corrosion protection of Al aerospace alloys. *J Coat. Technol. Res.* (2004), 1, 69-80.

5. Wicks, Z. W.; Jones, F. N.; Pappas, S. P.; Wicks, D. A., *Organic Coatings: Science and Technology*. Third ed.; John Wiley & Sons: Hoboken, 2007.

6. Shreepathi, S.; Bajaj, P.; Mallik, B. P., Electrochemical impedance spectroscopy investigations of epoxy zinc rich coatings: Role of Zn content on corrosion protection mechanism. *Electrochimica Acta* (2010), 55, 5129-5134.

7. Simões, A. M.; Battocchi, D.; Tallman, D. E.; Bierwagen, G. P., SVET and SECM imaging of cathodic protection of aluminium by a Mg-rich coating. *Corrosion Science* (2007), 49, 3838-3849.

8. Battocchi, D.; Simões, A. M.; Tallman, D. E.; Bierwagen, G. P., Electrochemical behaviour of a Mg-rich primer in the protection of Al alloys. *Corrosion Science* (2006), 48, 1292-1306.

9. Bierwagen, G.; Battocchi, D.; Simões, A.; Stamness, A.; Tallman, D., The use of multiple electrochemical techniques to characterize Mg-rich primers for Al alloys. *Progress in Organic Coatings* (2007), 59, 172-178.

10. Bierwagen, G.; Brown, R.; Battocchi, D.; Hayes, S., Active metal-based corrosion protective coating systems for aircraft requiring no-chromate pretreatment. *Progress in Organic Coatings* (2010), 67, 195-208.

11. Simões, A.; Battocchi, D.; Tallman, D.; Bierwagen, G., Assessment of the corrosion protection of aluminium substrates by a Mg-rich primer: EIS, SVET and SECM study. *Progress in Organic Coatings* (2008), 63, 260-266.

12. DeRosa, R. L.; Szabo, I.; Bierwagen, G. P.; Battocchi, D., The effect of exposure condition on the degradation behavior of magnesium rich coatings. *Progress in Organic Coatings* (2015), 78, 455-461.

13. Upadhyay, V.; Allahar, K. N.; Bierwagen, G. P., Environmental humidity influence on a topcoat/Mg-rich primer system with embedded electrodes. *Sensors and Actuators B: Chemical* (2014), 193, 522-529.

14. Wang, D.; Battocchi, D.; Allahar, K. N.; Balbyshev, S.; Bierwagen, G. P., In situ monitoring of a Mg-rich primer beneath a topcoat exposed to Prohesion conditions. *Corrosion Science* (2010), 52, 441-448.

15. King, A. D.; Birbilis, N.; Scully, J. R., Accurate Electrochemical Measurement of Magnesium Corrosion Rates; a Combined Impedance, Mass-Loss and Hydrogen Collection Study. *Electrochimica Acta* (2014), 121, 394-406.

16. Bierwagen, G.; Brown, R.; Battocchi, D.; Hayes, S., Active metal-based corrosion protective coating systems for aircraft requiring no-chromate pretreatment. *Progress in Organic Coatings* (2010), 68, 48-61.

17. Wang, J.; Xu, H.; Battocchi, D.; Bierwagen, G., The determination of critical pigment volume concentration (CPVC) in organic coatings with fluorescence microscopy. *Progress in Organic Coatings* (2014), 77, 2147-2154.

18. Wang, S. F.; Ogale, A. A., Continuum space simulation and experimental characterization of electrical percolation behavior of particulate composites. *Composites Science and Technology* (1993), 46, 93-103.

19. Chen, Y.; Pan, F.; Wang, S.; Liu, B.; Zhang, J., Theoretical estimation on the percolation threshold for polymer matrix composites with hybrid fillers. *Composite Structures* (2015), 124, 292-299.

20. Bertei, A.; Nicolella, C., Percolation theory in SOFC composite electrodes: Effects of porosity and particle size distribution on effective properties. *Journal of Power Sources* (2011), 196, 9429-9436.

21. Barletta, M.; Gisario, A.; Trovalusci, F.; Vesco, S., Visual appearance and scratch resistance of high performance thermoset and thermoplastic powder coatings. *Progress in Organic Coatings* (2013), 76, 244-256.

22. Puig, M.; Cabedo, L.; Gracenea, J. J.; Suay, J. J., The combined role of inhibitive pigment and organo-modified silica particles on powder coatings: Mechanical and electrochemical investigation. *Progress in Organic Coatings* (2015), 80, 11-19.

23. Deflorian, F.; Rossi, S.; Fedel, M.; Ecco, L. G.; Paganica, R.; Bastarolo, M., Study of the effect of corrosion inhibitors on powder coatings applied on steel. *Progress in Organic Coatings* (2014), 77, 2133-2139.

24. Foulon-Belkacemi, N.; Coelho, R., Conduction and charge-injection in polypropylene films aged by corona discharge with streamers. *Journal of Physics D: Applied Physics* (1995), 28.

25. Tsuchiya, Y.; Akutu, K.; Iwata, A., Surface modification of polymeric materials by atmospheric plasma treatment. *Progress in Organic Coatings* (1998), 34, 100-107.

26. Battocchi, D.; Bierwagen, G.; Stamness, A.; Tallman, D.; Simões, A., 5 - Magnesium-rich primers for chromate-free protective systems on Al 2024 and Al 7075. In *Innovative Pre-Treatment Techniques to Prevent Corrosion of Metallic Surfaces*, Fedrizzi, L.; Terryn, H.; Simões, L., Eds. Woodhead Publishing: 2007; pp 63-70.

27. Barletta, M.; Gisario, A.; Tagliaferri, V., Electrostatic spray deposition (ESD) of polymeric powders on thermoplastic (PA66) substrate. *Surface and Coatings Technology* (2006), 201, 296-308.

28. Ravindran, N.; Chattopadhyay, D. K.; Zakula, A.; Battocchi, D.; Webster, D. C.; Bierwagen, G. P., Thermal stability of magnesium-rich primers based on glycidyl carbamate resins. *Polymer Degradation and Stability* (2010), 95, 1160-1166.

29. Talbert, R., *Powder Coating*. Fifth ed.; The Chemical Coaters Association: Taylor Mill, 2009.

CHAPTER 3. PRELIMINARY INVESTIGATION ON THE EFFECT OF MAGNESIUM-RICH PRIMER ON THE FILM FORMATION AND BARRIER PROPERTIES OF FUSION BONDED EPOXY COATINGS

Abstract

In order to investigate compatibility and corrosion protection performance, powder coatings based on an epoxy-dicyandiamide (E-DICY) powder coating formulation was prepared and applied to AA-2024-T3 panels coated with Mg-rich primer (MgRP). The primers were applied to aluminum panels and allowed to cure before being topcoated by the powder coating, which was applied by a hot-dip fluidized bed technique. Visual and microscopic inspection of the dual coat protection system revealed the primer had no effect on the film formation of the powder topcoat. Panels topcoated with the E-DICY coating were exposed to constant immersion in 5% NaCl solution. Corrosion resistance by barrier protection was investigated by electrochemical impedance spectroscopy (EIS). The E-DICY topcoat exhibited outstanding barrier protection of the underlying metal substrate, and the presence of a MgRP underlayer did not appear to decrease the barrier performance of the topcoat.

Introduction

Fusion bonded epoxies (FBE) have become a favored organic coating for transmission pipes across the world with successful pipeline protection in extreme environments ranging from arctic regions in Canada to Saudi Arabian desert conditions [1-3]. Adding to the range of environments, these coatings are used as both internal and external applications of a variety of fluids, including aqueous media and petroleum products [3-4]. Performance properties of FBE systems depends on polymer network properties, adhesion to substrates, and resistance to abrasion by flowing media [5].

One of the more common crosslinking compounds used for FBE is dicyandiamide (DICY). Depending on cure temperature, the DICY hardener has been shown to react with epoxy systems by multiple mechanisms to create a highly crosslinked thermosetting polymer network [6]. For increased protection to electrolyte diffusion in transfer pipes, the coating is typically applied very thick, up to 500 μm [2]. Resistance to abrasion and erosion damage of the film is often accomplished by addition of hard minerals including silica [5]. When used in multilayer systems, the FBE is typically applied directly to the metal substrate, and functions as a primer with high barrier performance. Though barrier protection is an

effective means of limiting corrosion, time dependent diffusion of electrolyte or physical damage to the film will eventually lead to environmental attack and corrosion of the metal substrate.

Coating systems which employ FBE typically do not include additional primer or corrosion inhibiting layers. Often times, a secondary mechanism to corrosion protection is provided by an external impressed current system and sacrificial anodes. The metal structure is polarized to behave cathodically, forcing corrosion half-cell reduction reactions, and providing cathodic protection to the metal. Impressed current systems have been proven effective in protecting coated structures, but it is possible for accelerated corrosion reactions to cause premature delamination or cathodic disbondment of the coating [7]. The mechanism for cathodic disbondment is driven by reduction of water into hydroxide ions at the substrate-coating interface, creating alkaline conditions, and decreasing adhesion of the coating. In natural conditions, delamination is usually very slow, but in the presence of excess impressed current, the delmaination front can advance rapidly, resulting in failure of barrier properties of the coating [8].

Extensive work has been done at NDSU to develop magnesium-rich primers (MgRP) which, when applied to aluminum, have proven effective in providing cathodic protection to the aluminum metal [9-14]. There is much interest in combining FBE and MgRP coating to provide corrosion protection by multiple mechanisms. As a topcoat, FBE provides excellent barrier protection to underlying coatings and metal substrate. The presence of a MgRP layer beneath the topcoat could potentially increase the protective life of the FBE, without the need for external sacrificial anodes or impressed current systems. The following work was performed to determine the feasibility of combining MgRP and FBE to create a dual coat corrosion protection system for long-life protection of aluminum substrates.

Experimental

Powder Coat Preparation

In this study, an epoxy powder coating consistent with commercially-available pipeline topcoats was used. The coating was based on a solid bisphenol-A/epichlorohydrin epoxy resin cured with a DICY hardener. Weight fractions of the resin and crosslinker were 96/4 respectively. The formulation was filled with pigments and extenders at a 20% PVC of mineral charges, mainly silica and oxides of calcium and titanium. This powder formulation is referred to as E-DICY throughout this report.

Powder was prepared in batches of approximately four pounds. Raw material blends were made by combining resin, crosslinking agent, additives, and extenders to be premixed by manual agitation of all necessary materials. Material compounding was performed on a Prism TSE 24 twin-screw powder coat extruder at a temperature of 120°C and 200 rpms. After passing through chill rollers, the extrudate was collected and manually pulverized to dime-size chips. Grinding was performed with a MIKRO Bantam hammer and screen mill. Material collected after grinding was sieved on a SWECO vibratory screening separator with a 150 mesh sieve to collect particles smaller than 100 μm for the finished paint powder. Finished powder was verified for batch consistency by gel time and visual appearance.

Coating Application

Aluminum panels were prepared from 150x75x2 mm^3 AA 2024-T3 panels, supplied by Q Panel Lab Products. Bare panels were prepared by sandblasting with 80 μm alumina grit and degreased with hexanes. MgRP coated panels were prepared with 45% PVC MgRP as outlined in Chapter 2. Before powder topcoat application, panels were suspended in a preheated oven for 30 minutes with the oven set to 230°C. Powder was added to the fluidized bed hopper and the air supply was increased until the powder was properly fluidized. The powders were allowed 30 minutes of fluidization before any panels were coated. Coatings were applied by fully immersing the preheated panels into the fluidized powder for approximately two seconds to build proper film thickness. The coated panels were then removed from the fluidized powder and placed back in the oven for two minutes for complete cure. After curing, panels were removed from the oven and immediately quenched in a water bath. Samples prepared without primer had a topcoat film thickness of 300±10μm. Total thickness of the combined MgRP and epoxy topcoat films was 400±20 μm as determined by a Positector 6000 under non-ferrous conditions. Free films were prepared following a similar procedure with steel panels cut from a non-stick baking sheet. These panels were consistent in size with the aluminum test panels, and once cooled, these panels allowed for easy release of the cured free films.

Differential Scanning Calorimetry (DSC)

Thermal behavior and extent of cure was characterized by conventional differential scanning calorimetry (DSC) using a Q1000 DSC from TA Instruments. Samples were prepared from coating free films which had already been cured by the recommended cure schedule. Sample mass was

approximately 10 mg, and was tested in standard aluminum DSC pans. Before DSC experiments were performed, residual thermal stresses were relieved by conditioning the samples in an oven at 50°C for 30 minutes. In the DSC, Heat-Cool-Heat cycles were performed from 25ºC to 250ºC, at ramp rates of 20ºC/min for heating and 10ºC/min for cooling. Glass Transition Temperature (T_g) was recorded at the midpoint of the endothermic shift in the heat flow curve.

Dynamic Mechanical Analysis (DMA)

Dynamic mechanical analysis (DMA) was performed using a TA Instruments Q800 DMA to investigate thermal behavior of the materials. Samples were prepared as fully cured coating free films cut to approximately 25.4mm long by 5mm wide and 0.1 mm thick. The prepared samples were conditioned in an oven at 50ºC for 30 minutes to relieve any residual stresses. Experiments were run under strain-amplitude control of 0.01% with a preload force of 0.01 N and force track of 125%. Tests were conducted from room temperature to a final temperature of 200ºC at a ramp rate of 2ºC/min. A fixed frequency of 1 Hz was used for all tests. Measurement of storage modulus (E') and loss modulus (E") allowed for calculations of loss tangent (tan δ). The temperature at maximum tan δ was recorded as T_g. The E' at 60ºC above T_g was recorded as the rubbery plateau modulus (E_r), which was used to calculate crosslink density (υ) of the cured films by:

$$\upsilon = \frac{E_r}{3RT} \quad \text{(Eq. 3.1)}$$

where R is the universal gas constant (8.314 $cm^3PaK^{-1}mol^{-1}$) and T is absolute temperature (K). Due to pigment present in the system, crosslink density was calculated with Er modified by Einstein's equation [15-16]:

$$E = E_o(1 - 2.5\phi) \quad \text{(Eq. 3.2)}$$

where E is the elastic modulus of the pigmented coating, E_o is the modulus of the unpigmented coating, and ϕ is the pigment volume fraction.

Scanning Electron Microscopy (SEM)

Cross sectional microscopy was performed by a JEOL JSM-6490LV scanning electron microscope (SEM). Samples were prepared by cutting 2 cm x 2 cm square sections from prepared panels, and casting the samples in EpoFix epoxy casting resin. Upon hardeneing, the samples were polished on a Struers TegraPol-25 with a variety of polishing disks. Fully polished samples were finished

with an MD-Nap disk and DiaPro 1 µm water based diamond suspension. Polished samples were coated with a thin film of carbon for proper grounding and imaging in the SEM unit.

Electrochemical Impedance Spectroscopy (EIS)

Electrochemical Impedance Spectroscopy (EIS) studies were performed using Gamry Reference 600 Potentiostats with Gamry Framework Version 6.20/EIS300 data acquisition software. An electrolyte solution of 5% NaCl was used for all experiments and measurements were carried out in triplicates. Coatings applied to aluminum substrates were tested with a standard three electrode setup with a saturated calomel reference electrode, platinum mesh counter electrode, and the coated substrate as a working electrode. The electrochemical cell was contained by a glass cylinder clamped to the sample with an o-ring sealing the connection and preventing any leakage. The exposed area of the working electrode was 7.06 cm^3. Measurements were taken over a frequency range of 100,000-0.01 Hz with 10 collection points per frequency decade. An AC potential perturbation was applied at 10 mV RMS versus the open circuit potential of the system. All impedance data presented is normalized to 1 cm^2. Constant immersion samples were left uncovered at room temperature. Solution levels were monitored and, under the assumption that no salts would evaporate from the solutions, electrolyte levels were maintained by adding DI water until the original fill volume was achieved. At two week intervals the electrolyte solutions were flushed and replaced by new solution.

Results and Discussion

Characterization of Epoxy-Dicyandiamide Powder Coatings

Results from DSC, which measures change in heat flow with temperature change, are shown in Figure 3.1 below. A shift in heat flow is seen at 110°C, indicating glass transition of the polymer film. Above Tg, the heat flow curve remains linear for the remainder of the experiment, demonstrating full cure in the polymer film. Any chemical reactions occurring in the post-Tg temperature ramp would be indicated by endothermic or exothermic peaks in the curve. From these results, it is assumed the cure schedule of 2 minutes at 230°C, followed by a water quench, is sufficient for curing the epoxy powder coating.

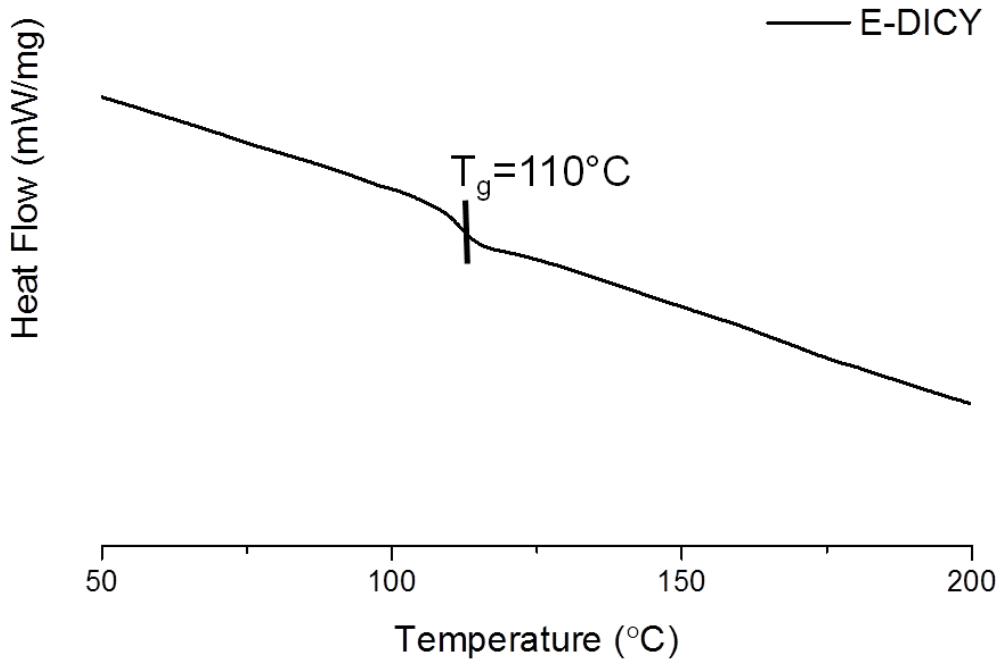

Figure 3.1. DSC results from a cured free film sample of E-DICY.

Changes in mechanical behavior at increasing temperatures were investigated by DMA. Plotted in Figure 3.2 are E' and tan δ curves from an E-DICY free film sample subject to temperatures between 50°C to 225°C. For comparison, the plot includes results from the polyester coating PTFF discussed in Chapter 2. The coating transitions from an amorphous glassy phase to a rubbery elastic phase over the range of 130°C to 160°C, with tan δ max indicating T_g at 144°C. Crosslink density was calculated from E' at T_g+60°C, where the film displayed stable rubbery elastic behavior. With E'=10.43 MPa at 204°C, crosslink density was calculated to be 5.84E-4 mol/cm^3. Additionally, no increase in E' was observed in the rubbery elastic state, indicating no further crosslinking took place.

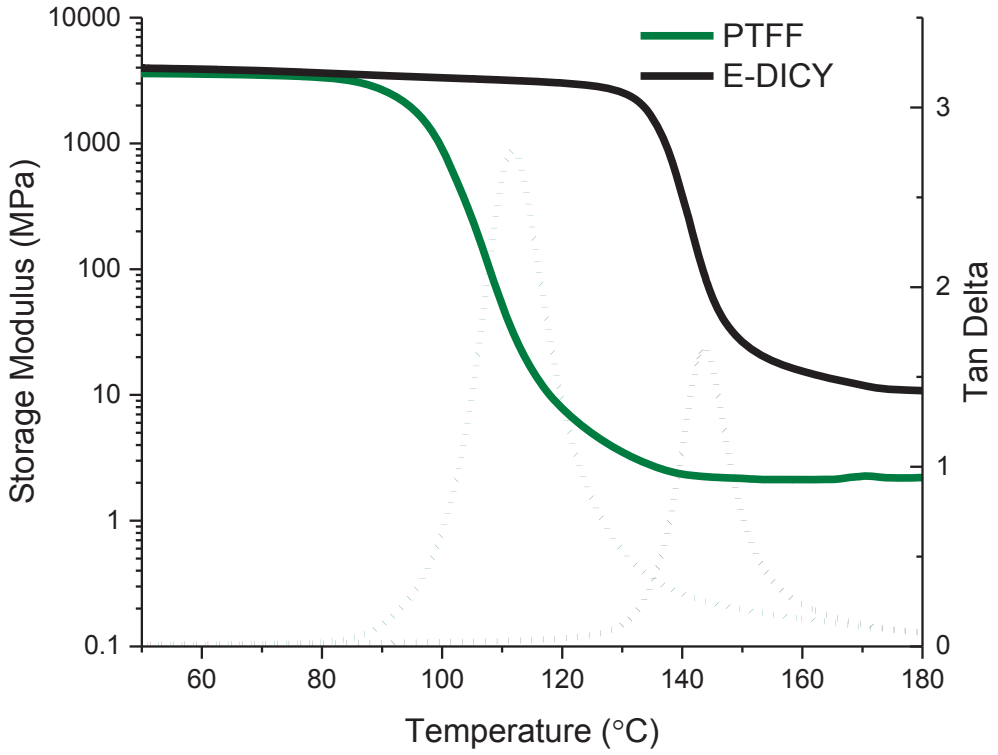

Figure 3.2. DMA results; comparison of E' and tanδ for E-DICY (black) and PTFF (green).

Application of an Epoxy-Dicyandiamide Coating to Mg-Rich Primer

Macroscopic surface finish can be seen in Figure 3.3. Under inspection by the naked eye, samples show no difference in surface characteristics. The epoxy topcoat used for these tests is a very robust system, relying on fast gel time and cure reactions to rapidly build film thickness when hot-dipped in a fluidized bed. Being as thick as they are, differences in surface roughness between sandblasted aluminum and MgRP do not appear to affect surface characteristics of the final film. Microscopic cross sectional images are shown in Figure 3.4. In the SEM images, microscopic details of the coating systems are revealed. Light colored inclusions in the topcoat film represent the pigments and extender dispersed in the polymer matrix. Topcoat films applied directly to sandblasted aluminum are observed to have a number of voids trapped in the film. This is to be expected in thermosetting systems that combine fast gel times with thick film build, as trapped gasses do not have sufficient time to degas before the crosslinked network is formed at gel point. This effect can be minimized by applying powder coats by electrostatic spray on preheated substrates, but the presence of voids or film porosity is not uncommon for high

temperature application of similar fusion bonded epoxies [17]. Topcoat film formation on MgRP does not appear significantly different than on sandblasted aluminum. Small voids are formed in the topcoat film, often near the MgRP surface, but a similar effect was evident in the topcoats applied to sandblasted aluminum. Though inherent defects are formed in the topcoat, the films are sufficiently thick that the voids should not play a significant role in decreasing the barrier properties of the coating system.

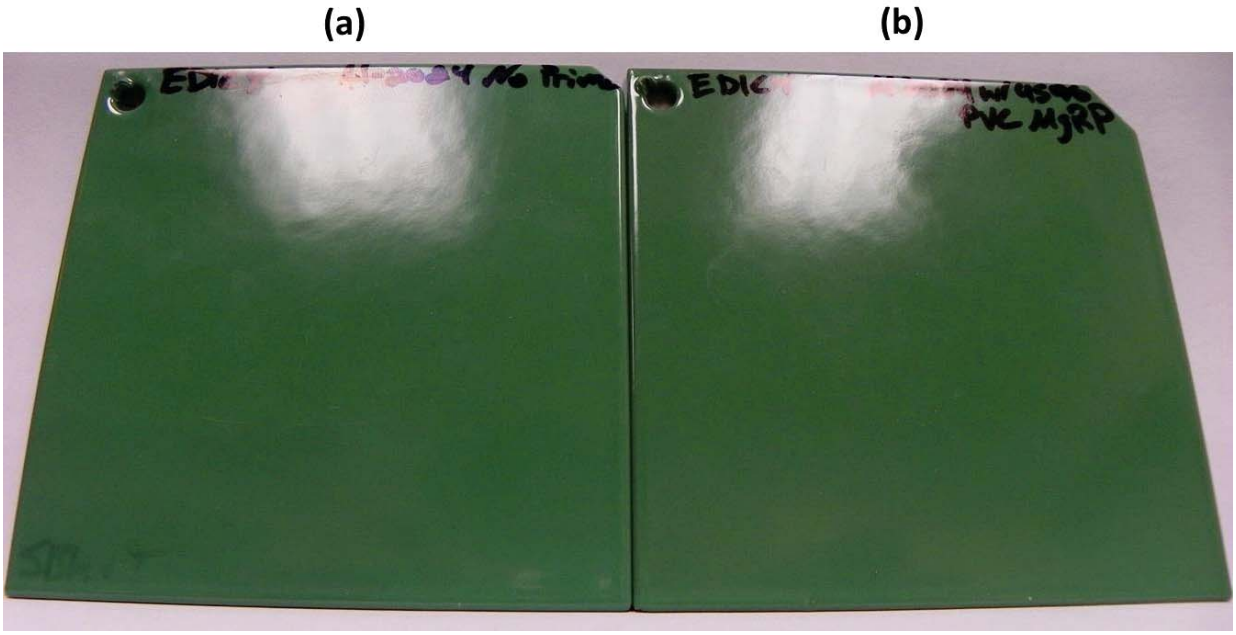

Figure 3.3. Images of panels coated with E-DICY including (a) no primer and (b) 45% MgRP.

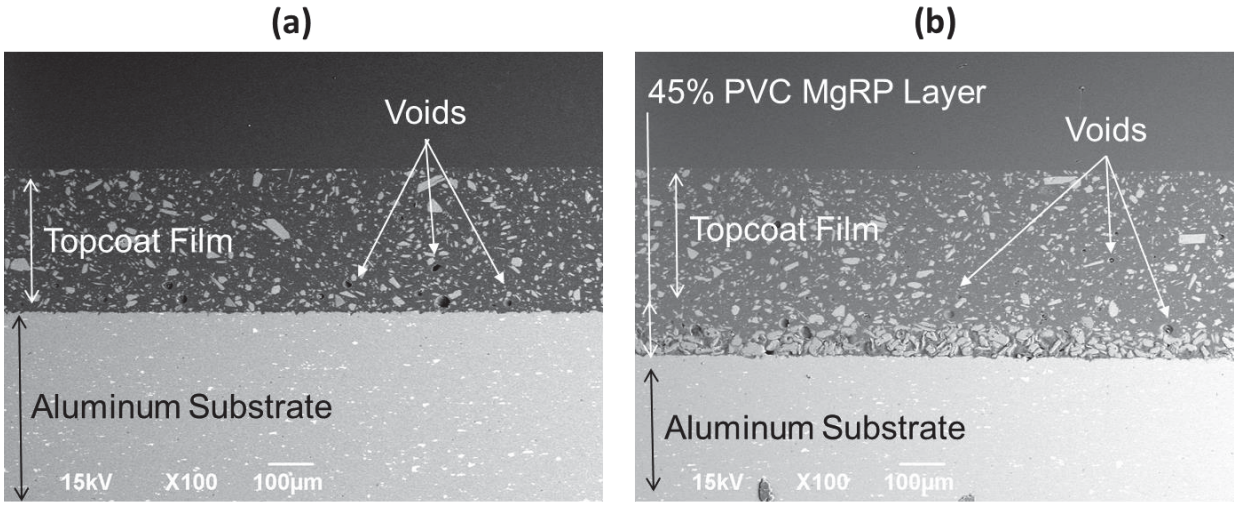

Figure 3.4. SEM images from sample cross sections with (a) no primer and (b) 45% MgRP.

Barrier Protection of the Dual-Coat System

Characterization of the barrier properties exhibited by the topcoated systems was done by EIS measurements. Topcoated panels with and without MgRP were subject to constant immersion in 5% NaCl. Results from a topcoated sample without primer are shown in Figure 3.5. At one hour of immersion the sample exhibits behavior that is largely capacitive, with a low frequency impedance near 100 GΩ and maximum phase angle of -70°, indicating some diffusion of electrolyte into the film. Experiments were run at intervals of approximately 200 hours, but due to a lack of characteristic changes, only curves from 4800 hours and 7000 hours of immersion are shown. Impedance decreases slightly due to water diffusion into the polymer film, but at less than one order of magnitude, the impedance change is very minimal considering immersion time. Results from topcoated samples that include a MgRP layer are also shown in Figure 3.5. Comparisons between samples with and without primer show no distinct differences over the lifetime of these tests. At up to 7000 hours constant immersion, the electrolyte has still not fully penetrated the topcoat to begin interactions at primer or substrate surfaces. For this time scale, the presence of MgRP does not appear to alter the barrier properties of the epoxy topcoat, which continues to function as an excellent barrier to electrolyte penetration.

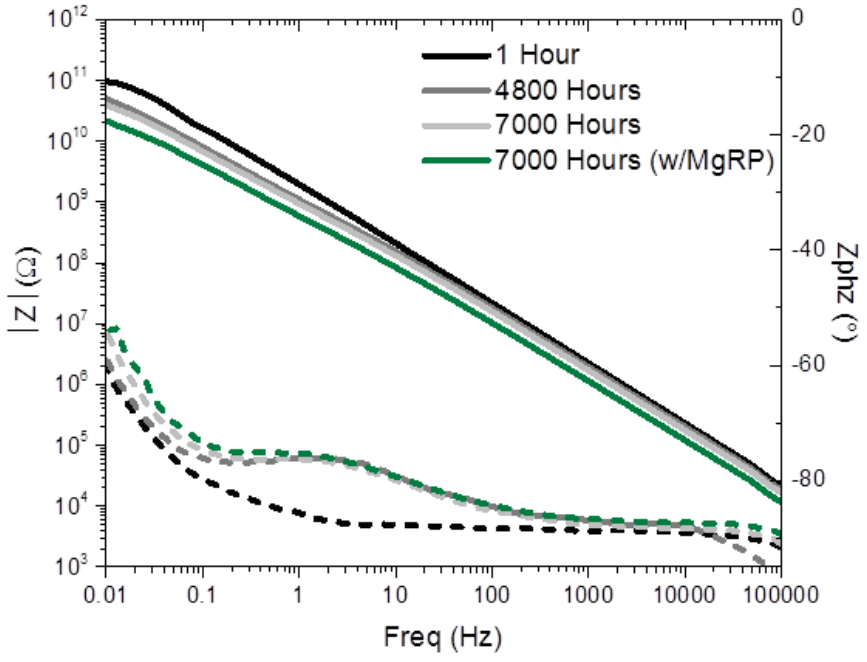

Figure 3.5. Bode impedance and phase curves for E-DICY up to 7000 hours constant immersion without primer (black/gray) and at 7000 hours with MgRP

Conclusions

An epoxy topcoat, crosslinked by a dicyandiamide hardener, was studied to determine physical structure and electrochemical barrier properties, along with topcoat compatibility with MgRP. DSC experiments were performed to verify the topcoats formed fully cured networks after their recommended cure schedule. Glass transition of the topcoat was found by DMA experiments to be 144°C. In the post-Tg range, rubbery elastic behavior was observed. Crosslink density was calculated from the storage modulus of the material in the rubbery elastic stage. After modifying modulus by Einstein's equation to eliminate pigment effects, the crosslink density was calculated to be 5.84E-4 mol/cm^3; this is approximately three times the crosslink density exhibited by polyester-TGIC topcoats studied in Chapter 2.

Cured film structure of the E-DICY topcoat was investigated by SEM. Images from the coating cross-sections revealed topcoat film formation to be similar regardless of the presence of an MgRP layer. In either case, the E-DICY film was formed with small voids in the film. EIS was performed on samples subject to constant immersion in 5% NaCl electrolyte. Results from EIS show no distinguishable difference between samples without primer versus those that included a MgRP film under the E_DICY topcoat. Over the duration of the 7000 hour immersion time, impedance of the coatings remained over 10 GΩ·cm^2. The topcoats maintained largely capacitive behavior with electrolyte diffusion into the films.

References

1. Fu, A. Q.; Cheng, Y. F., Characterization of the permeability of a high performance composite coating to cathodic protection and its implications on pipeline integrity. *Progress in Organic Coatings* (2011), 72, 423-428.

2. Malik, A. U.; Andijani, I.; Ahmed, S.; Al-Muaili, F., Corrosion and mechanical behavior of fusion bonded epoxy (FBE) in aqueous media. *Desalination* (2002), 150, 247-254.

3. Mobin, M.; Malik, A. U.; Andijani, I. N.; Al-Muaili, F.; Al-Hajri, M.; Ozair, G.; Mohammad, N. M. K., Performance evaluation of some fusion-bonded epoxy coatings under water transmission line conditions. *Progress in Organic Coatings* (2008), 62, 369-375.

4. Husain, A.; Al-Bahar, S.; Chakkamalayath, J.; Vikraman, A.; Al Ghamdi, A.; Kamshad, T.; Siriki, R. S., Differential scanning calorimetry and optical photo microscopy examination for the analysis of failure of fusion bonded powder epoxy internal coating. *Engineering Failure Analysis*.

5. Luo, S.; Zheng, Y.; Li, J.; Ke, W., Effect of curing degree and fillers on slurry erosion behavior of fusion-bonded epoxy powder coatings. *Wear* (2003), 254, 292-297.

6. Amdouni, N.; Sautereau, H.; Gérard, J.-F.; Pascault, J.-P., Epoxy networks based on dicyandiamide: effect of the cure cycle on viscoelastic and mechanical properties. *Polymer* (1990), 31, 1245-1253.

7. Mahdavian, M.; Naderi, R.; Peighambari, M.; Hamdipour, M.; Haddadi, S. A., Evaluation of cathodic disbondment of epoxy coating containing azole compounds. *Journal of Industrial and Engineering Chemistry* (2015), 21, 1167-1173.

8. Rohwerder, M.; Hornung, E.; Stratmann, M., Microscopic aspects of electrochemical delamination: an SKPFM study. *Electrochimica Acta* (2003), 48, 1235-1243.

9. Battocchi, D.; Simões, A. M.; Tallman, D. E.; Bierwagen, G. P., Electrochemical behaviour of a Mg-rich primer in the protection of Al alloys. *Corrosion Science* (2006), 48, 1292-1306.

10. Bierwagen, G.; Battocchi, D.; Simões, A.; Stamness, A.; Tallman, D., The use of multiple electrochemical techniques to characterize Mg-rich primers for Al alloys. *Progress in Organic Coatings* (2007), 59, 172-178.

11. Bierwagen, G.; Brown, R.; Battocchi, D.; Hayes, S., Active metal-based corrosion protective coating systems for aircraft requiring no-chromate pretreatment. *Progress in Organic Coatings* (2010), 67, 195-208.

12. DeRosa, R. L.; Szabo, I.; Bierwagen, G. P.; Battocchi, D., The effect of exposure condition on the degradation behavior of magnesium rich coatings. *Progress in Organic Coatings* (2015), 78, 455-461.

13. Nanna, M.; Bierwagen, G., Mg-rich coatings: A new paradigm for Cr-free corrosion protection of Al aerospace alloys. *J Coat. Technol. Res.* (2004), 1, 69-80.

14. Simões, A.; Battocchi, D.; Tallman, D.; Bierwagen, G., Assessment of the corrosion protection of aluminium substrates by a Mg-rich primer: EIS, SVET and SECM study. *Progress in Organic Coatings* (2008), 63, 260-266.

15. Einstein, A., Eine neue Bestimmung der Moleküldimensionen. *Annalen der Physik* (1906), 324, 289-306.

16. Perera, D. Y., Effect of pigmentation on organic coating characteristics. *Progress in Organic Coatings* (2004), 50, 247-262.

17. Jadoon, A. N. K.; Thompson, I., Fusion bonded epoxy mainline and field joint coatings performance from the X100 field trial – A case study. *International Journal of Pressure Vessels and Piping* (2012), 92, 48-55.

CHAPTER 4. SUMMARY

Various powder topcoat chemistries were investigated for thermal behavior, network properties, and barrier protection in constant electrolyte immersion. Formulations varied by crosslink chemistry and pigment volume concentration. Thermosetting polyester powder topcoats were prepared based on either TGIC or HAA hardeners. TGIC crosslinked coatings have long served as superdurable topcoats, but toxicity concerns have led to restricted use. Designed to be substituted in for TGIC, HAA crosslinking agents have been developed to offer a more environmentally friendly option.

Topcoat lifetime and barrier protection is very different for each of these systems. When applied to AA-2024-T3, the TGIC crosslinked topcoats were able to maintain barrier protection beyond 4000 hours constant immersion in 5% NaCl electrolyte. Over the duration of exposure, impedance values for the TGIC systems remained in excess of 10 $G\Omega \cdot cm^2$. Though electrolyte was observed to diffuse into the films, the TGIC crosslinked coatings never developed a significant pore resistance. The presence of pigments and extenders exhibited little effect on the overall performance properties of the polyester-TGIC topcoats. Systems crosslinked by HAA hardeners displayed a much shorter time to failure under similar conditions. Polyester-HAA model coatings were fully penetrated by electrolyte within 1000 hours of constant immersion. Over 4000 hours of immersion the impedance was decreased by four orders of magnitude, resulting in failed barrier protection. Polyester-HAA topcoats failed at higher rates with the formulation that included pigments and extenders. Overall, barrier protection provided by the polyester topcoats appeared closely related to mechanical properties and crosslink density of the films.

Proof of concept was provided for application of powder topcoats to MgRP. Topcoat film formation was consistent between panels with and without MgRP when applied by electrostatic spray to preheated panels. Initial experiments showed no compatibility issues between MgRP and polyester powder topcoats when applied by the hot spray technique. When the powder topcoat is applied to MgRP on preheated panels, the topcoat film formation is consistent with topcoated panels without primer underlayers. The topcoat film is capable of forming without significant voids in the film, while the surface appearance maintains a smooth glossy appearance. When applied successfully over MgRP, the polyester topcoat is capable of providing corrosion protection by barrier performance. Combining MgRP with the polyester topcoat creates a protective system capable of inhibiting corrosion in three stages.

Initially, the topcoat provides high barrier protection, limiting electrolyte penetration through the film. In the presence of topcoat film defects, the MgRP first provides cathodic protection to any exposed aluminum substrate. Additionally, consumption of magnesium by sacrificial corrosion releases Mg ions into the electrolyte. Cathodic reactions at sites of exposed aluminum create alkaline conditions, which cause precipitation of magnesium oxides at the substrate surface. The resulting oxide layer is capable of providing barrier protection to the previously exposed metal substrate.

The compatibility between MgRP and Fusion Bonded Epoxy (FBE) was also explored. FBE is often used for rugged applications in extremely harsh environments. Although these coatings are extremely durable, they are often incompatible with other protective coatings systems. This equates to a systems that relies heavily on the protective properties of a single protective film, which can lead to rapid failure of the substrate when the FBE is damaged. When applied by the hot-dip fluidized bed technique, the epoxy powder showed no differences in film formation on sandblasted aluminum or MgRP surfaces. Impedance of the FBE coated systems remained over 10 $G\Omega \cdot cm^2$ after 7000 hours of constant immersion in 5% NaCl electrolyte, with no noticeable differences between coating systems with or without MgRP. These preliminary results indicate the FBE and MgRP systems are compatible when applied as dual coat protective coatings.

CHAPTER 5. FUTURE WORKS

The work presented in this report is intended to provide a solid baseline for future research on corrosion protection systems combining MgRP and powder topcoats. Proof of concept was provided for applying powder topcoats to MgRP, and initial performance of the system was verified. There is still much work that remains in characterizing these combined systems over increased exposure times. Long-term constant immersion of samples with powder topcoats applied to MgRP will help determine the increases in service life provided by the combined coating systems. Additional tests should include other exposure environments and the effects of film defects. The effects of defect size are particularly interesting. There is much to be learned as far as the “throwing power”, or effective distance from the MgRP layer that an aluminum substrate would remain protected by cathodic protection. Scanning probe techniques, including SVET and SECM, would provide critical details to the effects of cathodic protection induced by the MgRP.

The actual mechanism of failure for the polyester-HAA topcoats should be further explored. Compared to TGIC crosslinked topcoats, the HAA systems exhibit much faster times to failure. Results from water absorption tests showed an eventual decrease in weight gained due to water immersion. Currently, the cause of weight loss is not understood. A number of possibilities exist, including leaching of small molecule additives or pigments, or even the degradation of the crosslinked polyester network by hydrolysis of the polyester chains.

Long-term protection provided by FBE/MgRP dual coat systems should be continued to provide a complete understanding of the failure mechanism and duration of corrosion protection provided by these combined systems. Additional compatibility investigations must include the effects of artificial film defects in the FBE topcoat, along with the effectiveness of MgRP to provide cathodic protection to the metal substrate.

Optimization of the MgRP by addition of conductive polymer nanospheres was an additional goal of the project, but was left for future researchers to investigate. Addition of conductive polymers, specifically polypyrrole (PPy), to the MgRP formulations has the potential to increase conductivity of the primer film. In turn, this could potentially increase effectiveness of the cathodic protection provided by the primer, while possible decreasing the concentration of Mg while maintaining efficient corrosion protection.